RESEARCH ACTIVITIES V
Department of Applied Molecular Science

V-A Molecular Mechanisms of Oxygen Activation by Heme Enzymes

By sharing a common prosthetic group, the heme enzymes such as cytochrome P450s, peroxidases, and catalases catalyze their own unique biological functions; monooxygenation, hydrogen peroxide dependent oxidation, and dismutation of hydrogen peroxide, respectively. Our efforts have been focused on the elucidation of the structure-biological function relationship of thoses heme enzymes by employing both enzymic systems including mutants and their model systems.

V-A-1 Investigations of the Myoglobin Cavity Mutant H93G with Unnatural Imidazole Proximal Ligands as a Modular Peroxide O-O Bond Cleavage Model System

ROACH, Mark P.; OZAKI, Shin-ichi[1]; WATANABE, Yoshihito
([1]Yamagata Univ.)

[*Biochemistry* **39**, 1446 (2000)]

A general inability to carry out extensive variations in the electronic characteristics of proximal heme iron ligands in heme proteins has hampered efforts to obtain a clear understanding of the role of the proximal heme iron ligand in the activation of oxygen and peroxide. The disadvantage of the frequently applied site directed mutagenesis technique is that it is limited by the range of natural ligands available within the genetic code. The myoglobin cavity mutant H93G has its proximal histidine ligand replaced by glycine, a mutation which leaves an open cavity capable of accommodation of a variety of unnatural potential proximal ligands. We have carried out investigations of the effect of changing the electron donor characteristics of a variety of substituted imidazole proximal ligands on the rate of formation of myoglobin compound II and identified a correlation between the substituted imidazole N-3 pK_a (which provides a measure of the electron donor ability of N-3) and the apparent rate of formation of compound II. A similar rate dependence correlation is not observed upon binding of azide. This finding indicates that O–O bond cleavage and not the preceding peroxide binding step is being influenced by the electron donor characteristics of the substituted imidazole ligands. The proximal ligand effects are clearly visible but their overall magnitude is quite low (1.7 fold increase in O–O bond cleavage rate per pK_a unit). This appears to provide support for recent commentaries that the partial ionization of the proximal histidine ligand in typical heme peroxidases may not be enough of an influence to provide a mechanistically critical push effect. Further attempts were made to define the mechanism of the influence of N-3 pK_a on O–O bond cleavage by using peracetic acid and cumene hydroperoxide as mechanistic probes. The observation of heme destruction in these reactions indicates that displacement of the proximal imidazole ligands by peracetic acid or cumene hydroperoxide has occurred. A combination mutation; H64D/H93G was prepared with the objective of observing compound I of H64D/H93G with substituted imidazoles as proximal ligands upon reaction with H_2O_2. This double mutant was found to simultaneously bind imidazole to both axial positions, an arrangement which prevents a reaction with H_2O_2.

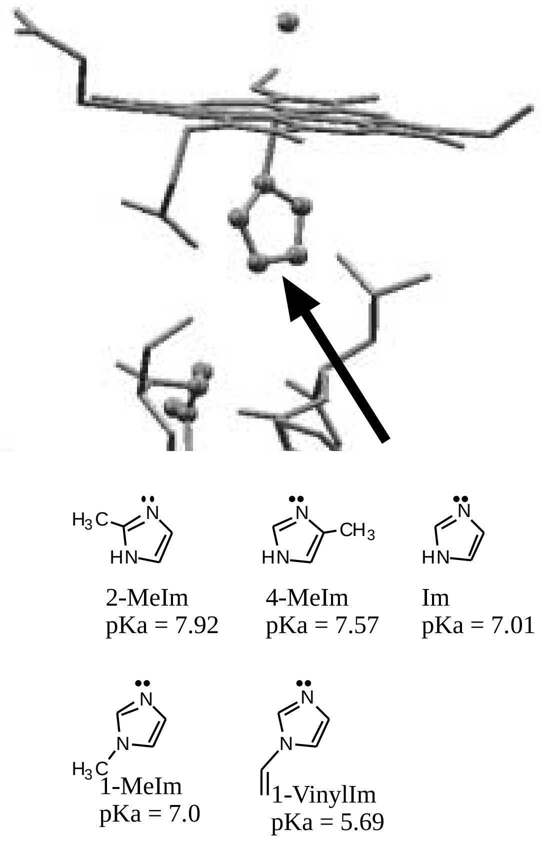

Figure 1. Active site of the ferric imidazole adduct of H93G Mb. Also shown are the five Im-X used as proximal ligands for H93G and their pK_a values

V-A-2 Formation and Catalytic Roles of Compound I in the Hydrogen Peroxide-Dependent Oxidations by His64 Myoglobin Mutants

MATSUI, Toshitaka; OZAKI, Shin-ichi; WATANABE, Yoshihito

[*J. Am. Chem. Soc.* **121**, 9952 (1999)]

A His64 → Asp mutant of sperm whale myoglobin (Mb), H64D Mb, has been prepared to mimic the active site of chloroperoxidase from the marine fungus *Caldariomyces fumago*, in which distal glutamic acid is suggested to enhance the compound I formation by H_2O_2. The H64D mutant allows us to see the accumulation of compound I in the reaction of Mb with H_2O_2 for the first time. The successful observation of compound I is due to at least 50-fold improvement in the formation rate of compound I as well as its stabilization upon the His64 → Asp replacement. Catalytic activity of wild type Mb and a series of His64 Mb mutants (H64A, H64S, H64L, and H64D Mb) are examined for one-electron oxidation and oxygenation by using H_2O_2 as an oxidant. The H64D mutant is the best catalyst among the myoglobins and shows 50~70-fold and 600~800-fold higher activity than the wild type in the one-electron oxidations and peroxygenations, respectively. The origin of the varied activity upon the mutations is discussed on the basis of the formation rate and stability of compound I.

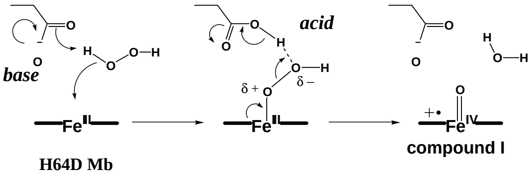

Scheme 1. Roles of distal aspartate of H64D myoglobin in the reaction with H_2O_2.

V-A-3 Proximal Ligand Control of Heme Iron Coordination Structure and Reactivity with Hydrogen Peroxide: Investigations of the Myoglobin Cavity Mutant H93G with Unnatural Oxygen Donor Proximal Ligands

ROACH, Mark P.; PUSPITA, Waheeda J.; WATANABE, Yoshihito

[*J. Inorg. Biochem.* **81**, 173 (2000)]

The role of the proximal heme iron ligand in activation of hydrogen peroxide and control of spin state and coordination number in heme proteins is not yet well understood. Although there are several examples of amino acid sidechains with oxygen atoms which can act as potential heme iron ligands, the occurrence of protein-derived oxygen donor ligation in natural protein systems is quite rare. The sperm whale myoglobin cavity mutant H93G Mb (Barrick, D. *Biochemistry* **33**, 6546 (1994)) has its proximal histidine ligand replaced by glycine, a mutation which leaves an open cavity capable of accommodation of a variety of unnatural potential proximal ligands. This provides a convenient system for studying ligand-protein interactions. Molecular modeling of the proximal cavity in the active site of H93G Mb indicates that the cavity is of a sufficient size to accommodate benzoate and phenolate in conformations that allow their oxygen atoms to come within binding distance of the heme iron. In addition, benzoate may occupy the cavity in an orientation which allows one carboxylate oxygen atom to ligate to the heme iron while the other carboxylate oxygen is within hydrogen bonding distance of serine 92. The ferric phenolate and benzoate complexes have been prepared and characterized by UV-visible and MCD spectroscopies. The benzoate adduct shows characteristics of a six-coordinate high-spin complex. To our knowledge, this is the first known example of a six-coordinate high-spin heme complex with an anionic oxygen donor proximal ligand. The benzoate ligand is displaced at alkaline pH and upon reaction with hydrogen peroxide. The phenolate adduct of H93G Mb is a five-coordinate high-spin complex whose UV-visible and MCD spectra are distinct from those of the histidine 93 to tyrosine (H93Y Mb) mutant of sperm whale myoglobin. The phenolate adduct is stable at alkaline pH and exhibits a reduced reactivity with hydrogen peroxide relative to that of both native ferric myoglobin, and the exogenous ligand free derivative of ferric H93G Mb. These observations indicate that the identity of the proximal oxygen donor ligand has an important influence on both the heme iron coordination number and the reactivity of the complex with hydrogen peroxide.

V-A-4 Mechanisms of Sulfoxidation Catalyzed by High-Valent Intermediates of Heme Enzymes: Electron Transfer *vs.* Oxygen Transfer Mechanism

GOTO, Yoshio; MATSUI, Toshitaka; OZAKI, Shin-ichi[1]; WATANABE, Yoshihito; FUKUZUMI, Shunichi[2]
([1]Yagata Univ.; [2]Osaka Univ)

[*J. Am. Chem. Soc.* **121**, 9497 (1999)]

The mechanism of sulfoxidation catalyzed by high-valent intermediates of heme enzymes has been studied by direct observation of the reduction of compounds I of HRP (horseradish peroxidase) and His64Ser myoglobin (Mb) mutant as well as $O=Fe^{IV}TMP^{+\bullet}$ (**1**) (TMP = 5,10,15,20-tetramesitylporphyrin dianion) by sulfides. The reaction of thioanisole and compound I of HRP (10 μM, pH 7.0, 298K) gives the resting state of HRP with accumulation of compound II as an intermediate. The yield of sulfoxide by a stoichiometric reaction of HRP compound I with thioanisole was only 25 ± 5%. On the other hand, the same sulfoxidation by both **1** and His64Ser Mb compound I exclusively exhibited two-electron process resulting in quantitative formation of sulfoxide. When 1,5-dithiacyclooctane (DTCO) is employed as a substrate, the reaction of His64Ser Mb compound I with DTCO exhibits rapid formation of compound II which decays to the ferric state due to the low oxidation potential of DTCO. The observed rate constants (log k) of the reactions of **1** and compounds I of HRP and His64Ser Mb with a series of p-substituted thioanisoles correlate with the one-electron oxidation potentials (E^0) of the sulfides. A comparison of these correlations with the established correlation between log k and E^0 for the corresponding electron transfer reactions of substituted *N*,*N*-dimethylanilines has revealed that the reactions of compound I of HRP with the sulfides proceed via electron transfer while that the sulfoxidation of sulfides by **1** and compound I of His64Ser Mb occurs via direct oxygen transfer rather than electron transfer.

V-B Model Studies of Non-Heme Proteins

Non-heme proteins play important roles in biological redox processes. Many reactions catalyzed by the non-heme enzymes are quite similar to those by hemoproteins. We are interested in the active intermediates responsible for oxidation and oxygenation by non-heme enzyme, especially the similarity and differences.

V-B-1 A Bis(μ-oxo)dicopper(III) Complex with Aromatic Nitrogen Donors: Structural Characterization and Reversible Conversion between Copper(I) and Bis(μ-oxo)dicopper(III) Species

HAYASHI, Hideki[1]; FUJINAMI, Shuhei[1]; NAGATOMO, Shigenori; OGO, Seiji; SUZUKI, Masatatsu[1]; UEHARA, Akira[1]; WATANABE, Yoshihito; KITAGAWA, Teizo
([1]Kanazawa Univ.)

[*J. Am. Chem. Soc.* **122**, 2124 (2000)]

It is important to explore how the nature of donor atoms and the stereochemistry of ligands influence the structures and properties of bis(μ-oxo)dicopper(III) complexes. In this context, we have synthesized a bis(μ-oxo)dicopper(III) complex, $[Cu_2(O)_2(Me_2\text{-tpa})_2tpa](PF_6)_2 \cdot 2(CH_3)_2CO$ (**1b**), having a tetradentate tripodal ligand containing aromatic nitrogen donors. The most striking feature of **1b** is the reversible conversion with a precursor copper (I) complex $[Cu(Me_2\text{-tpa})]^+$ (**1a**) in CH_2Cl_2 at –80 °C by bubbling N_2 gas. Such reversible behavior has not been observed for the bis(μ-oxo)-dicopper(III) complexes. Thus reactivity patterns in copper–dioxygen chemistry significantly vary with ligand system. Me_2-tpa has a unique ability to stabilize both copper(I) and copper(III) oxidation states: it can take not only a square planar structure having weak ligation from the axial positions suitable for formation of copper (III) oxidation state but also a pyramidal structure sitable for formation of copper(I) oxidation state.

V-B-2 Characterization of Imidazolate-Bridged Cu(II)-Zn(II) Heterodinuclear and Cu(II)-Cu(II) Homodinuclear Hydroperoxo Complexes as Reaction Intermediate Models of Cu, Zn-SOD

OHTSU, Hideki[1]; ITOH, Shinobu[2]; NAGATOMO, Shigenori; KITAGAWA, Teizo; OGO, Seiji; WATANABE, Yoshihito; FUKUZUMI, Shunichi[1]
([1]Osaka Univ.; [2]Osaka City Univ.)

[*Chem. Commun.* 1051 (2000)]

Copper-zinc superoxide dismutase (Cu, Zn-SOD) contains an imidazolate-bridged Cu(II)-Zn(II) heterodinuclear metal center in its active site. This enzyme catalyses a very rapid two-step dismutation of superoxide to dioxygen and hydrogen peroxide through an alternate reduction and oxidation of the active-site copper ion. An outer-sphere electron transfer from superoxide to Cu(II) center occurs to produce O_2 and Cu(I) center which may be oxidized by another molecule of superoxide in the presence of proton to produce H_2O_2 via a hydroperoxo-Cu(II) species. The hydroperoxo-copper(II) species is a key intermediate in biological oxidations catalyzed by copper enzymes including SOD. We report herein the first characterization of SOD model hydroperoxo-Cu(II) intermediates generated by the reactions of hydrogen peroxide with the imidazolate-bridged Cu(II)-Zn(II) heterodinuclear and Cu(II)-Cu(II) homodinuclear complexes.

V-B-3 Synthesis and X-ray Crystal Structure of a Novel Mn(II)-Semiquinonate Complex $[Mn^{II}(TPA)(DTBSQ)]BPh_4$, and Its Dioxygenase-like Activity: Relevance to Manganese(II)-Dependent Catechol Dioxygenases

FUNABIKI, Takuzo[1]; OGO, Seiji; ITO, Tomoyuki[1]; MATSUI, Hajime[1]; YAMAMOTO, Takashi[1]; TANAKA, Tsunehiro[1]; HOSOKOSHI, Yuko; MAKIHARA, Nobuyuki; WATANABE, Yoshihito
([1]Kyoto Univ.)

Catechol dioxygenases play key roles in the metabolism of various aromatic compounds, converting aromatics to aliphatics with insertion of molecular oxygen between a C–C bond of a benzene ring, and have been studied extensively in recent years from both sides of enzymes and models. We here report synthesis of a novel Mn(II)-semiquinonate complex, $[Mn^{II}(TPA)(DTBSQ)]X$ (**1**, DTBSQ: 3,5-di-tert-butyl-1,2-benzosemiquinonate; TPA: tris(2-pyridylmethyl)amine; X: Cl or BPh_4), that is oxygenated with molecular oxygen in the intradiol cleavage fashion. The complex is a new type of mononuclear mono(3,5-di-tert-butyl-1,2-benzosemiquinonate)manganese(II) complex, and highly peculiar not only for the electronic configuration keeping the Mn(II) state even after coordination of a semiquinonate radical anion, but also for the geometric configuration that is not in the usual octahedral geometry.

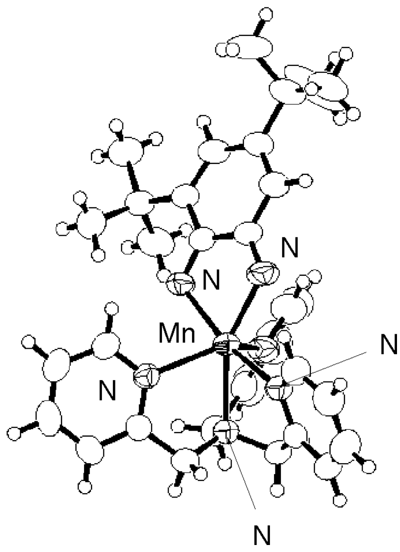

Figure 1. ORTEP drawing of **1**.

V-B-4 Infrared Spectroscopic Features of the Cyclic Hydrogen-Bonded *cis*(Hydroxo)–Fe^{III}–(Carboxylato) Unit of Lipoxygenase Active Site Models

OGO, Seiji; YAMAHARA, Ryo^1; ROACH, Mark P.; AKI, Michihiko; OGURA, Takashi^2; KITAGAWA, Teizo; MASUDA, Hideki^1; WATANABE, Yoshihito
(^{1}Nagoya Inst. Tech. and IMS; ^{2}Univ. Tokyo)

[submitted for publication]

Lipoxygenases (LOs) are mononuclear non-heme iron enzyme which are widely distributed among plants and mammals. LOs catalyze the peroxidation of polyunsaturated fatty acids containing the *cis,cis*-1,4-diene moiety to the corresponding 1-hydroperoxy-*trans,cis*-2,4-diene. This paper reports infrared (IR) spectroscopic features of the structurally characteristic *cis*(hydroxo)–Fe^{III}–(carboxylato) unit of lipoxygenase active site model complexes, [Fe^{III}(tnpa)(OH)(RCO$_2$)]-ClO$_4$ (**1a**: R = CH_3 and **1b**: R = H). The vibrational modes were unequivocally assigned by isotopic substitution of the hydroxo ($^{18}OH^-$, $^{16}OD^-$, and $^{18}OD^-$ for $^{16}OH^-$) and the carboxylato (**1a**: $^{12}CH_3{}^{12}C^{18}O_2^-$, $^{13}CH_3{}^{12}C^{16}O_2^-$, $^{12}CH_3{}^{13}C^{16}O_2^-$, and $^{13}CH3^{13}C^{16}O_2^-$ for $^{12}CH_3{}^{12}C^{16}O_2^-$ and **1b**: $H^{13}C^{16}O_2^-$ for $H^{12}C^{16}O_2^-$) ligands in the solid state (in mineral oil) and in the liquid state (in acetonitrile). The crystal structure of **1a** was determined by X-ray analysis. It was confirmed by electrospray ionization mass spectrometry (ESI-MS) that the structures of the complexes are preserved in acetonitrile.

V-C Aqueous Organometallic Chemistry

In recent years, aqueous organometallic chemistry has been widely studied because of industrial advantages and environmental concerns. Few organometallic aqua complexes have been, until now, isolated and used as water-soluble reagents in aqueous media. We have investigated a homogeneous hydrogenation in aqueous media using organometallic aqua complexes whose structures and properties drastically change as a function of pH because of deprotonation of the aqua ligands.

V-C-1 pH-Selective Hydrogenation with an Organometallic Aqua Complex as a Catalyst Precursor in Very Acidic Media

MAKIHARA, Nobuyuki; OGO, Seiji; WATANABE, Yoshihito

[*Organometallics* in press]

An organometallic aqua complex [Cp*Ir^{III}(H$_2$O)$_3$]$^{2+}$ (**1**) serves as a catalyst precursor for aqueous hydrogenation of water-soluble compounds with C=O or C=C bonds under very acidic conditions. The hydrogenation shows unique pH-selectivity depending upon substrates. The rates of hydrogenation of carbonyl compounds show a maximum in a pH range of about 2 to 3. The rates of hydrogenation of water-soluble alkenes show a maximum in a pH range of about –1 to 2. Above pH 4, complex **1** is deprotonated to form a catalytically inactive dinuclear complex [(Cp*Ir^{III})$_2$(μ-OH)$_3$]$^+$ (**2**). This is the first example of a pH-selective hydrogenation using an organometallic aqua complex as the catalyst precursor under very acidic conditions.

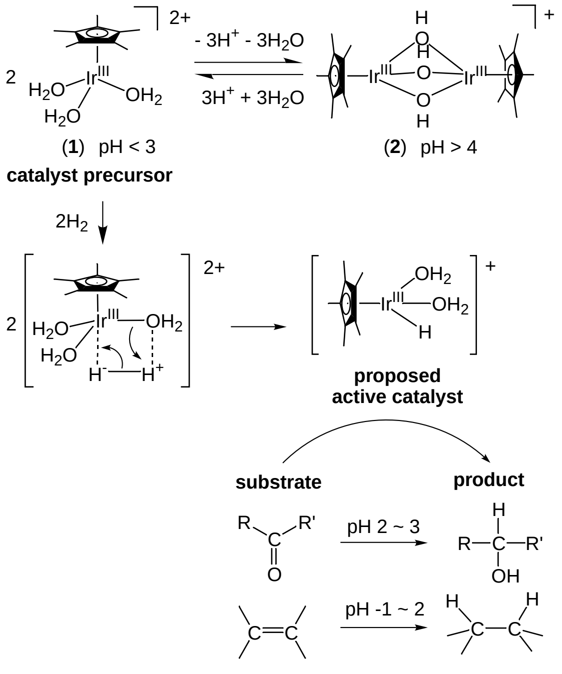

Scheme 1. pH-Selective hydrogenation with an organo-metallic aqua complex.

V-D Magnetic Structure of Oligo-Nitroxide-Transition Metal Complexes

Since one or two decades, considerable attention has been devoted to stable nitroxide radicals and their metal complexes which are now widely used as building blockes for the design of moleculaer-based magnetic materials. In this field, we have introduced a new strategy of employing π-conjugated polyaminoxyls as ligands in which the 2*p*-spins of the NO groups interact ferromagnetically ($J_1 > 0$). The dimensionality of the complex and the sign and magnitude of the exchange coupling between the neighboring spins may be readily tuned by this strategy. Depending on the nature of the additional interchain or interlayer interaction, the polymers are expected to become an antiferromagnet or ferri/ferromagnet. By modifying and extending this design strategy to bis- and tris(aminoxyl) radicals having triplet and quartet ground states, respectively, we have been able to construct with the aid of magnetic metal ions one-dimensional (1D) chain, two-dimensional (2D) network and three-dimensional (3D) parallel-crosses structures in which both the organic 2p and metallic 3d spins have been ordered in macroscopic scales. Since such a rational approach by self-assembly to the tailored extended systems having relevant physical properties is of great importance in materials synthesis. For these materials, the magnetic structures of the crystals are also interesting.

V-D-1 Influence of the Thermal Excitations of the Ferrimagnetic (–1/2,5/2,–1/2) Linear Trimer on the Paramagnetic Behavior of the Layered Metal-Radical Complex $\{Mn(hfac)_2\}_3(R_X)_2 \cdot n\text{-}C_7H_{16}$

MARKOSYAN, Ashot S.[1]**; HOSOKOSHI, Yuko; INOUE, Katsuya**
([1]IMS and Moscow State Univ., Russia)

[*Phys. Lett. A* **261**, 212 (1999)]

The complex $\{Mn(hfac)_2\}_3(\mathbf{3R}_\Delta)_2 \cdot n\text{-}C_7H_{16}$ forms a two-dimensional honeycomb-like spin network. It is shown that the spins of Mn(II) form with the two 1/2-spins of different adjacent triradicals $\mathbf{3R}_\Delta$ linear $(\bar{1}/2,5/2,\bar{1}/2)$ ferrimagnetic trimers, which determine the paramagnetic properties of the complex. The intratrimer excitations result in the decay of the trimers above 140 K. The experimental data can well be described within this model both at high and low temperatures thus proving the importance of the thermal excitations within the trimers. The best agreement was obtained at J_{TR}/k = –176.4 K and λ' = +0.333 emu/mol. The power series expansion for the 2D honeycomb network gives J_{TR}/k = –175.4 K and J_1/k = +0.226 K.

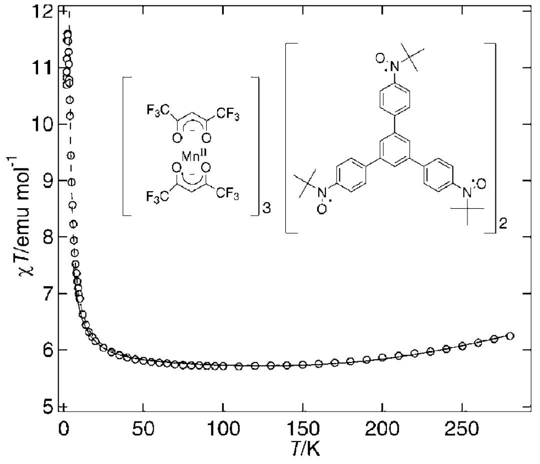

Figure 1. The temperature dependence of $\chi_m T$ for the layered complex $\{Mn(hfac)_2\}_3(\mathbf{3R}_\Delta)_2 \cdot n\text{-}C_7H_{16}$. Open circles are the experimental data, the solid and the dashed lines are the least squares fits for a 2D and 3D lattice, respectively.

V-D-2 Synthesis and Magnetic Properties of Bis(hexafluoroacetylacetonate) Copper(II) Complex with 5-Bromo-1,3-Phenylenebis(*N-tert*-butylaminoxyl) as a Bridging Ligand

IWAHORI, Fumiyasu; INOUE, Katsuya; IWAMURA, Hiizu[1]
([1]Kyushu Univ.)

[*Mol. Cryst. Liq. Cryst.* **334**, 533 (1999)]

Bis(hexafluoroacetylacetonato)copper(II), $Cu(hfac)_2$ (= M) reacts with 5-bromo-1,3-phenylenebis(*N-tert*-butylaminoxyl), $\mathbf{1}_{Br}$ to yield a complex of formula $[M_3 \cdot (\mathbf{1}_{Br})_2]$. The X-ray crystal structure shows that it crystallize in the space group *P*1, with a = 12.469(2) Å, b = 15.278(2) Å, c = 11.602(2) Å, α = 104.59(1)°, β = 111.86(1)°, γ = 88.32(1)°, and Z = 1. The crystal contains copper(II) trinuclear structure, M-$\mathbf{1}_{Br}$-M-$\mathbf{1}_{Br}$-M. The magnetic susceptibility measurements revealed a structual transition at *ca.* 48 K accompanied by a temperature hysterisis. (Figure 1)

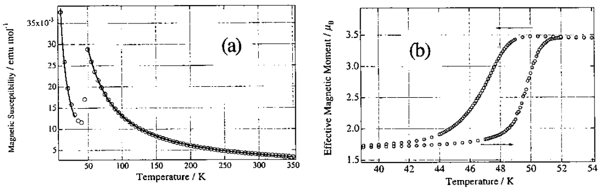

Figure 1. (a) χ_m versus T plot for $[Cu(hfac)_2]_3(\mathbf{1}_{Br})_2$ measured at a magnetic field of 50000 Oe; (b) Observed μ_{eff} versus T plots in the temperature range 39–45 K. Solid lines are calculated on Curie-Weiss law (15–45 K) and the trinuclear complex model (50–350 K).

V-D-3 Magnetic Behaviour of the Ferrimagnetic (–1/2,5/2,–1/2) Linear Trimer in Complexes of $Mn(hfac)_2$ with Bis- and Trisnitroxide Radicals

MARKOSYAN, Ashot S.[1]**; IWAMURA, Hiizu**[2]**; INOUE, Katsuya**
([1]IMS and Moscow State Univ., Russia; [2]Kyushu Univ.)

[*Mol. Cryst. Liq. Cryst.* **334**, 549 (1999)]

Characterization and magnetic properties of new metal-radical complexes with bivalent Mn having a general formula $\{[\mathrm{Mn(hfac)_2}]_m(\mathbf{R})_n\}$ are given. (Figure 1) In these complexes, the aminoxyl radicals have magnetic, triplet or qualtet, ground state and form with Mn^{2+} heterospin structures. They show 1D, 2D, and 3D behaviour depending on the crystal structure, chemical formula and molecular structure of radical. In the ordered state, the complexes form a ferrimagnetic structure due to a strong nagetive coupling between the radical and Mn spins. Magnetic anisotropy in some single crystal was studied. The 3D complex $\{[\mathrm{Mn(hfac)_2}]_3(\mathbf{3R}_\mathrm{T})_2\}$ with a linear triradical can be described within a sublattice model of ferrimagnetism, one sublattice of which os formed by 1D chains, while the other consists of magnetically isolated Mn^{2+} ions. Its comparatively high T_C = 45 K is accounted for the large interchain exchange interaction (3.9 K) through the isolated Mn^{2+}.

Analysis of their paramagnetic properties shows that the hagher energy excitations are related to the desintegration of the ferrimagnetic (–1/2,5/2,–1/2) linear trimer species, which can be isolated in all these compounds.

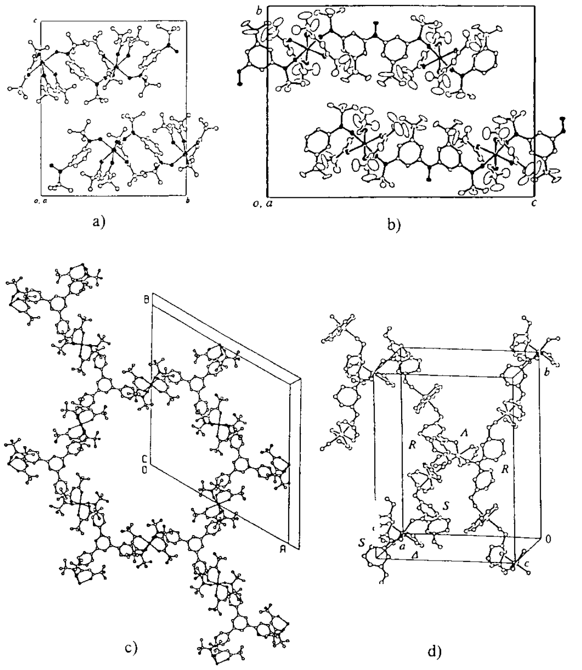

Figure 1. 1D chains of $\{[\mathrm{Mn(hfac)_2}](\mathbf{2R})\}$ extending along *b*-axis (a); an enatiomeric pair of isotactic 1D chains of $\{[\mathrm{Mn(hfac)_2}](\mathbf{3R}_\mathrm{T})\cdot n\text{-}\mathrm{C_6H_{14}}\}$ (the molecules of $n\text{-}\mathrm{C_6H_{14}}$ are disordered and not shown for clarity) (b); 2D hexagonal net of $\{[\mathrm{Mn(hfac)_2}]_3(\mathbf{3R}_\Delta)_2\cdot n\text{-}\mathrm{C_7H_{16}}\}$ viewed down to the *c*-axis (the $n\text{-}\mathrm{C_7H_{16}}$ molecules are not shown) (d); 3D parallel-crossed structure of $\{[\mathrm{Mn(hfac)_2}]_3(\mathbf{3R}_\mathrm{T})_2\}$ (the $\mathrm{CF_3}$ and $\mathrm{(CH_3)_2C}$ groups are not shown.

V-D-4 Exchange Coupling Parameters and Energy Levels for Cyclic Metal-Radical Complexes of Bis(hexafluoroacetylacetonato) manganese(II) with 5-*tert*-butyl-1,3-phenylenebis(*N*-*tert*-butyl-aminoxyl) and (4-*N*-*tert*-butyl-*N*-oxyamino)pyridine

RABU, Pierre[1]; DRILLON, Marc[1]; IWAMURA, Hiizu[2]; GÖITZ, Gunter[2]; ITOH, Tetsuji[2]; MATSUDA, Kenji[2]; KOGA, Noboru[2]; INOUE, Katsuya

([1]Inst. Phys. Chim. Matér. Strasbourg, France; [2]Kyushu Univ.)

[*Eur. J. Inorg. Chem.* **211**, 216 (2000)]

Temperature-dependant paramagnetic susceptibility data for two cyclic dimer complexes of bis(hexafluoroacetylacetonato)manganese (II) with 5-*tert*-butyl-1,3-phenylenebis(*N*-*tert*-butylaminoxyl) **1** and 4-(*N*-*tert*-butyl-*N*-oxyamino)pyridine have been analyzed to obtain two sets of two intermolecular exchange coupling parameters J_1 and J_2. (Figure 1, Scheme 1) A previous model, based on one of these interractions being much weaker than the other, could not be explicitly correlated to these actual exchange-coupling paramaters. However, the energy levels of the low lying spin states were found to be reproduced reasonably well by the approximate method.

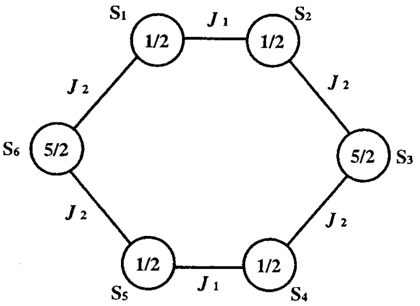

Scheme 1. A cyclic arrangement of the spins in $[\mathrm{Mn(hfac)_2}\cdot\mathbf{1}]_2$.

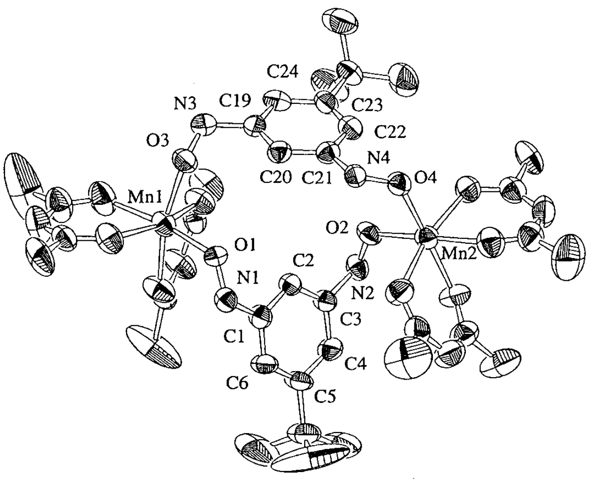

Figure 1. Structure of the cyclic complex $[\mathrm{Mn(hfac)_2}\cdot\mathbf{1}]_2$; Fluorine atoms, *N*-*tert*-Butyl groups and hydrogene atoms are omitted for clarity; thermal ellipsoids are drawn at the 50% probability level.

V-D-5 Synthesis and Magnetic Properties of a New Complex Made up of $\mathrm{Mn(hfac)_2}$ and a Radical with a Triplet Ground State

KUMAGAI, Hitoshi; HOSOKOSHI, Yuko; MARKOSYAN, Ashot S.[1]; INOUE, Katsuya

([1]IMS and M.V. Lomonosov Moscow State Univ.)

[*New J. Chem.* **24**, 537 (2000)]

A new metal-radical complex of Mn(II) made up of Mn(hfac)$_2$ and the radical 4-*N*-*tert*-butylaminoxyl-4'-(1-oxyl-3-oxide-4,4,5,5-tetramethylimidazolin-2-yl)-biphenyl (BIPNNNO) was synthesized. The X-ray single crystal structural analysis revealed that the complex consists of discrete molecules [Mn(hfac)$_2$]·(BIPNNNO)$_2$. The magnetic characteristics of this complex were studied and the Mn–radical and intraradical exchange integrals were evaluated: –135 ± 10 K and 72 ± 5 K, respectively. These values are compared with those of complexes of Mn(hfac)$_2$ with different aminoxyl polyradicals.

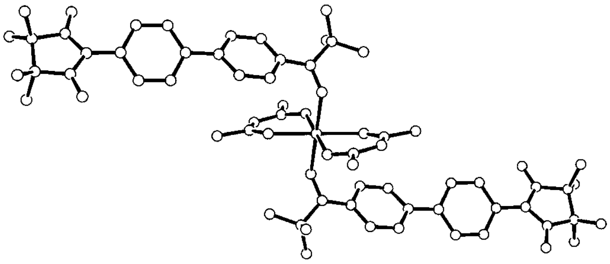

Figure 1. View of the discrete structure of Mn(hfac)$_2$-(BIPNNNO)$_2$.

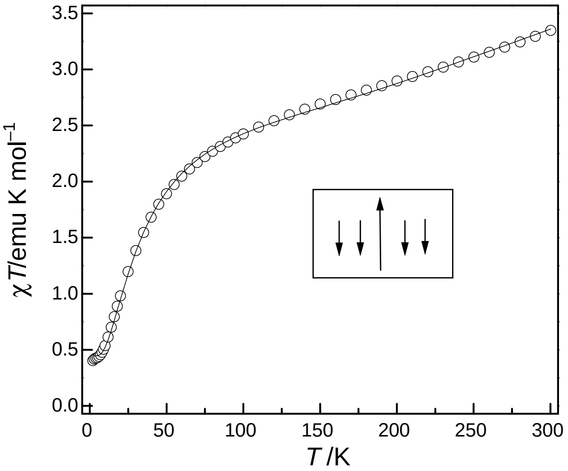

Figure 2. Temperature dependence of $\chi_m T$ of the complex Mn(hfac)$_2$(BIPNNNO)$_2$. The experimental data are shown by symbols and the solid line is the theoretical fit. The spin scheme of the complex is drawn in the frame.

V-D-6 Two-Dimensional Complexes of the General Formula [Mn(hfac)$_2$]$_3$·(R)$_2$ with Variable Metal-Radical Exchange Interactions

TANAKA AKITA, Motoko; HOSOKOSHI, Yuko; MARKOSYAN, Ashot S.[1]; IWAMURA, Hiizu[2]; INOUE, Katsuya

([1]IMS and M.V. Lomonosov Moscow State Univ.; [2]Kyushu Univ)

[*J. Phys. Chem.* submitted]

Magnetic properties of a series of new layered metal-nitroxide polyradical complexes with the general formula [M(hfac)$_2$]$_3$($\mathbf{R}_\Delta$)$_2$, M = Mn(II) or Cu(II), are studied. In these complexes the radicals have a quartet ground state and contribute essentially in magnetism. Several exchange interactions, between M and the NO group of the radical, the intraradical NO–NO interactions, are responsible in forming the magnetic properties of these heterospin systems. Depending on the character of the interlayer chemical bonds, they show either ferro/ferrimagnetic or antiferromagnetic long range order. The hirerachry of the different exchange interactions is established and the Mn–NO and Cu–NO exchange integrals are evaluated from analysis of the temperature dependence of the paramagnetic susceptibility. With increasing intraradical exchange interaction, the complexes exhibit a clear 2D behavior.

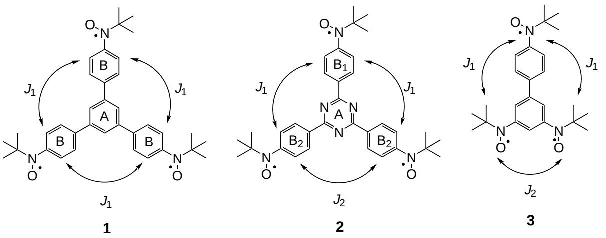

Figure 1. Triangular triradicals **1**, **2** and **3** with three ligating sites. A and B indicate the aromatic rings in different positions.

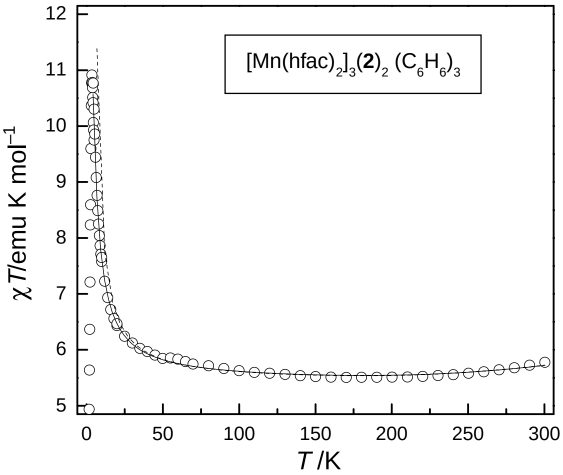

Figure 2. The temperature dependence of the product $\chi_m T$ for the complex [Mn(hfac)$_2$]$_3$(**2**)$_2$·(C$_6$H$_6$)$_3$. Open circles are the experimental data. The solid and the dot lines are the theoretical fits in the 2D and 3D models, respectively.

V-E Synthesis of Chiral Molecule-Based Magnets

The design of molecular materials with interesting magnetic and optical or electrical properties is one of the major challenges in the last few years. The synthesis and study of chiral molecular-based magnetic materials which are transparent for light are of great interest. Novel magneto-optical phenomena have been theoretically predicted and observed in chiral paramagnetic materials in 1997. Although novel properties are expected for such compounds, few examples of chiral molecular-based magnetic materials are still known. To get more insight in their properties it is therefore important to construct such chiral molecule-based magnets in a systematic way. We designed and synthesized a chiral organic radical which was can be employed to construct chiral molecular-based magnets.

V-E-1 Synthesis and Characterization of a Chiral Molecule-Based Metamagnet Made by a Chiral Triplet Organic Radical and Transition Metal Ion

KUMAGAI, Hitoshi; INOUE, Katsuya

[*Mol. Cryst. Liq. Cryst.* **334**, 487 (1999)]

Crystals of $\{\mathbf{1}\cdot\mathrm{M(II)(hfac)_2}\}_n$ (M = Mn, Cu) were obtained by mixing the 1,3-bis(*N*-*tert*-butylamino-*N*-oxyl)-5-{1-methyl-1-((*S*)-2-methylbutoxy)ethyl}-benzene (**1**) and bis(hexafluoroacetylacetonato)M(II) $\{\mathrm{M(II)\cdot(hfac)_2}\}$ in diethyl ether/*n*-heptane. A single crystal of $\{\mathbf{1}\cdot\mathrm{Mn(II)(hfac)_2}\}_n$ is triclinic, space group $P1$ (No. 1), with a = 11.0005(3) Å, b = 11.8183(4) Å, c = 17.7135(7) Å, α = 81.607(3)°, β = 84.801(3)°, γ = 63.516(2)°, V = 2038.3(1) Å^3, and D_X = 1.380 g/cm^3 for Z = 1. A single crystal of $\{\mathbf{1}\cdot\mathrm{Cu(II)(hfac)_2}\}_n$ is triclinic, space group $P1$ (No. 1), with a = 11.2831(7) Å, b = 11.5615(7) Å, c = 18.0163(9) Å, α = 82.384(4)°, β = 74.242(4)°, γ = 61.826(5)°, V = 1993.9(2) Å^3, and D_X = 1.43 g/cm^3 for Z = 1. An X-ray crystal structure analysis revealed the formation of a helical one-dimensional polymeric structure. It not only contains a (*S*) chiral carbon center but also (*R*) C2 chiral skeleton of the 1,3-bis(*N*-*tert*-butylamino-*N*-oxyl)benzene moiety. Each of the two aminoxyl radical centers are coupled ferromagnetically within the organic radical molecule and is coupled antiferromagnetically to the d^5 manganese(II) ions. The temperature dependence of the magnetization revealed that the heterospin system behaves as a metamagnet below 5.4 K. (Figure 1)

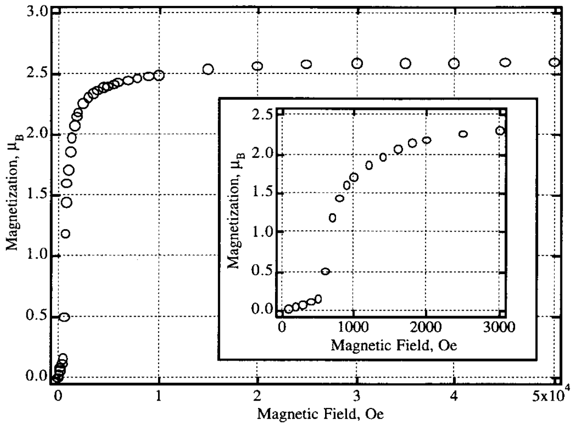

Figure 1. Field dependence of the magnetic moment at 1.8 K. Inset shows magnetic field range of 0 to 3000 Oe.

V-E-2 Synthesis, Structure and Magnetic Properties of a Chiral One-Dimensional Molecule-Based Magnet

KUMAGAI, Hitoshi; MARKOSYAN, Ashot S.[1]**; INOUE, Katsuya**
([1]IMS and Moscow State Univ., Russia)

[*Mol. Cryst. Liq. Cryst.* **343**, 97 (2000)]

A novel chiral organic radical 2-{4'-((*S*)-2''-methylbutoxy)phenyl}-4,4,5,5-tetramethylimidazoline-1-oxyl-3-oxide (**1**) and its metal complex, $[\mathbf{1}\cdot\mathrm{Mn(II)(hfac)_2}]_n$ were synthesized and characterized. The radical **1** crystallizes in the orthorhombic space group $P2_12_12_1$ (No. 19) with a = 11.494(3) Å, b = 25.328(3) Å, c = 6.1281(5) Å, V = 1748.0(4) Å^3. The complex $[\mathbf{1}\cdot\mathrm{Mn(II)(hfac)_2}]_n$ crystallizes in the same space group with a = 14.081(1) Å, b = 15.940(1) Å, c = 16.075(1) Å, V = 3608.1(4) Å^3. X-ray crystal structure analysis of the complex revealed the formation of a helical-chain structure. (Figure 1) The oxygen atoms of the radical **1** are ligated to two different manganese ions in cis position and exhibit the Δ configuration in $[\mathbf{1}\cdot\mathrm{Mn(II)(hfac)_2}]_n$. The magnetic measurements revealed that this chiral complex behaves as a ferrimagnet below T_C = 4.5 K. It is characterized by a strong intrachain exchange correlation, the ratio between the intrachain and interchain exchange interactions being about 10^{-5}.

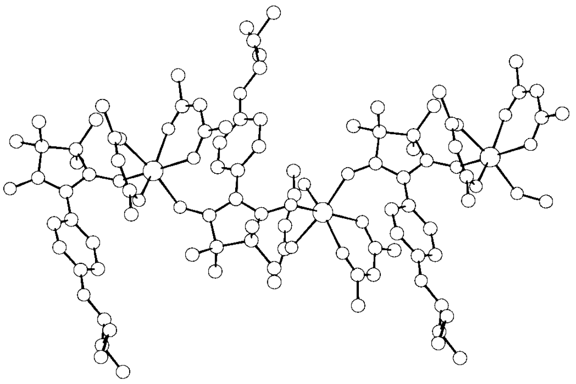

Figure 1. The X-ray crystal structure of the complex of $[\mathbf{1}\cdot\mathrm{Mn(II)(hfac)_2}]_n$. Hydrogene atoms and fluorine atoms are omitted for clarity.

V-F Synthesis and Characterization of Quantum-Spin Systems

There has been considerable current interest in the study of a low-dimensional quantum-spin system with an energy gap. Organic radicals suit such study, since they consist only of light elements and form ideal Heisenberg spin systems. By the appropriate design of molecules, we can obtain a variety of Heisenberg spin systems. As S = 1/2 antiferromagnetic lattices, we have synthesized a frustrated double chain system with an energy gap. Moreover, we have developed the study of intermediate state between S = 1/2 and S = 1. We have synthesized novel S = 1 species made of organic biradicals, having strong intramolecular exchange couplings of $2J/k_B$ ~ 200–700 K ($H = -2J\boldsymbol{S}_i \cdot \boldsymbol{S}_j$). Connection of the S = 1 molecules by the intermolecular antiferromagnetic exchange couplings in the crystalline state, leads to the intermediate state between S = 1/2 and S = 1. Adding to these, we focus on the ladder system, which is interesting in terms of Haldane state and the high T_C superconductivity. For the S = 1/2 Heisenberg spin ladder with antiferromagnetic legs and rungs, the ground state of the resonating valence bond (RVB) state or the dimerized state is theoretically expected. Experimentally, the singlet ground state was observed in some ladder systems formed by Cu-based compounds. The study of spin ladder systems has been mainly devoted to that of S = 1/2, but that of S = 1 is also interesting. For the ground state of the S = 1 ladder with antiferromagnetic legs ($J_{\|}$) and rungs ($J_{\perp}$), the Haldane state is expected in the extreme limit of $J_{\perp} \rightarrow 0$, and the dimer state in $J_{\|} \rightarrow 0$. In its ground state phase diagram on the $J_{\|}/J_{\perp}$ versus the energy gap (Δ), the phase transition from the dimer state to the Haldane state through a gapless point can be expected. A similar behavior of an existence of a gapless point between two different phases with their own finite excitation gaps is known for the S = 1 Heisenberg alternating antiferromagnetic chain system.

V-F-1 Construction of a Quantum-Spin System of *S* = 1/2 Antiferromagnetic Chain with the Next-Nearest-Neighbor Interactions

HOSOKOSHI, Yuko; KATOH, Keiichi; INOUE, Katsuya; GOTO, Tsuneaki[1]
([1]ISSP, Univ. Tokyo)

[*J. Phys. Soc. Jpn.* **68**, 2910 (1999)]

We have succeeded in synthesizing a new compound of a railroad trestle model, *i.e.*, a zigzag chain with next-nearest-neighbor interactions, having energy gap above the singlet ground state. We have synthesized novel organic radicals F_2PIMNH and Cl_2PIMNH, where F_2PIMNH = 2-[4'-*N*-*tert*-butylamino-2',6'-difluorophenyl]-4,4,5,5-tetramethyl-4,5-dihydro-1*H*-imidazol-1-oxyl and Cl_2PIMNH = 2-[4'-*N*-*tert*-butylamino-2',6'-dichlorophenyl]-4,4,5,5-tetramethyl-4,5-dihydro-1*H*-imidazol-1-oxyl. Both crystals include zigzag uniform chains made of hydrogen bondings. The magnetism of Cl_2PIMNH is explained by a uniform chain model with $2J_1/k_B = -3.4$ K and gapless ground state is suggested. On the other hand, the temperature dependence of χ_p in F_2PIMNH shows a maximum at around 3.4 K, and the χ_p values decrease rapidly below this temperature and goes exponentially to zero as $T \rightarrow 0$. Singlet ground state of this material is suggested. The magunitude of the energy gap, Δ = 3.1 K, was estimated by fitting the data below 2.4 K with the expression of $\chi \propto \exp(-\Delta/T)$. Comparison of the crystal structure between F_2PIMNH and Cl_2PIMNH, suggests that only F_2PIMNH has significant exchange coupling between the next-nearest-neighbors. The next nearest contact in F_2PIMNH is much shorter than the one in Cl_2PIMNH. There is theoretical expectation for the energy gap in the Heisenberg antiferromagnetic chain with the next-nearest-neighbor interaction. F_2PIMNH studied here is the first example of this model exhibiting an energy gap.

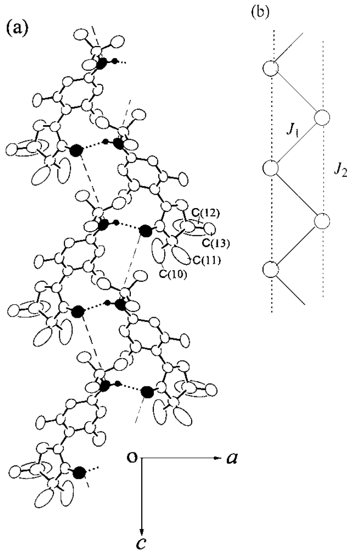

Figure 1. (a) Crystal structure of F_2PIMNH. (b) Scheme of the magnetic interactions in F_2PIMNH.

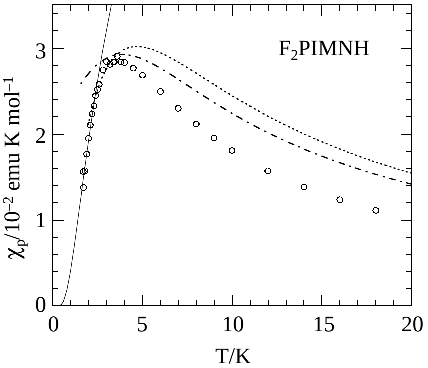

Figure 2. Temperature dependence of χ_p of F_2PIMNH. The solid curve is the fit of $\chi \propto \exp(-\Delta/T)$ with Δ = 3.1 K. The dotted broken curve is the calculation for the uniform chain with $2J/k_B = -6$ K, the interchain interactions by the mean-field treatment of $2zJ'/k_B$ = -5.2 K are adopted. The dotted curve represents the calculation for the alternating chain with $2J/k_B = -7.9$ K and $2zJ'/k_B = -6.3$ K.

V-F-2 Magnetic Properties of Low Dimensional Quantum Spin Systems Made of Stable Organic Biradicals PNNNO, F$_2$PNNNO and PIMNO

HOSOKOSHI, Yuko; NAKAZAWA, Yasuhiro; INOUE, Katsuya; TAKIZAWA, Kohichi[1]; NAKANO, Hiroki[1]; TAKAHASHI, Minoru[1]; GOTO, Tsuneaki[1]
([1]ISSP, Univ. Tokyo)

[*Phys. Rev. B* **60**, 12924 (1999)]

Stable organic biradical crystals PNNNO, F$_2$PNNNO and PIMNO of the PNNNO family were synthesized. (PNNNO = 2-[4’-(*N*-*tert*-butyl-*N*-oxyamino)phenyl]-4,4,5,5-tetramethyl-4,5-dihydro-1*H*-imidazol-1-oxyl 3-oxide, F$_2$PNNNO = 2-[2’,6’,-difluoro-4’-(*N*-*tert*-butyl-*N*-oxyamino)phenyl]-4,4,5,5-tetramethyl-4,5-dihydro-1*H*-imidazol-1-oxyl 3-oxide, PIMNO = 2-[4’-(*N*-*tert*-butyl-*N*-oxyamino)-phenyl]-4,4,5,5-tetramethyl-4,5-dihydro-1*H*-imidazol-1-oxyl.) All the molecules have strong intramolecular ferromagnetic exchange couplings to form $S = 1$ species. Depending on the molecular structure, the magnitude of the exchange coupling varies with $2J/k_B \sim$ 200–700 K. Both crystals of PNNNO and F$_2$PNNNO include similar chain structure formed by the contacts between the nitronyl nitroxide units. However, the magnetic behaviour is quite different from each other. The difference is attributed to the interchain interactions. Only F$_2$PNNNO has short contacts between the *N*-*tert*-butyl nitroxides as interchain interactions. The different interchain molecular arrangements are related to the difference in the molecular structure. There are noticeable difference in the dihedral angles between the benzene ring and radical planes owing to the electrostatic repulsion between the fluorine atoms and oxygen atoms on radical units. The interchain interactions in F$_2$PNNNO dominate the magnetism of this compound. The temperature dependence of the susceptibility suggests the existence of the energy gap above the singlet ground state. Moreover, the magnetization isotherm at low temperature exhibits a plateau at half the value of the saturation magnetization. These properties are quite rare among higher-dimensional spin systems than one-dimensional ones. Our theoretical calculation gives a qualitatively good explanation for the observed results.

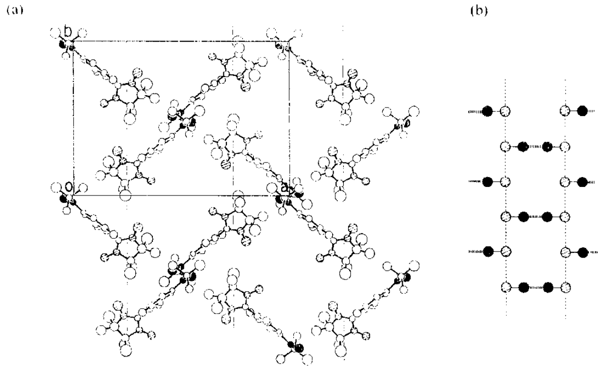

Figure 1. (a) Crystal structure of F$_2$PNNNO projected on the *ab* plane. *Pbca*, $a = 19.857$, $b = 14.010$, $c = 13.481$ Å, $V = 3750.5$ Å^3, $Z = 8$. Black and shaded ellipses represent the *N*-*tert*-butyl nitroxide and nitronyl nitroxide, respectively. (b) Schematic display of the crystal structure of F$_2$PNNNO. Black and shaded circles are correspond to the *N*-*tert*-butyl nitroxide and nitronyl nitroxide, respectively. Solid and broken lines represent the exchange path of the intra- and intermolecular interactions, respectively.

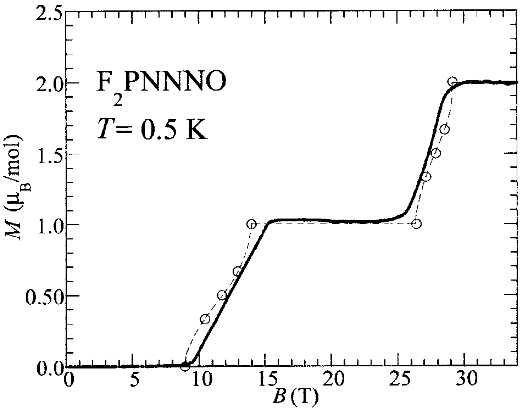

Figure 2. Magnetization process of F$_2$PNNNO at 0.5 K. Circles represent the calculated results.

V-F-3 Singlet Ground States in an Organic S = 1/2 Spin Ladder and a Novel Double Spin Chain of Ferromagnetic Dimers Formed by an Organic Tetraradical

KATOH, Keiichi; HOSOKOSHI, Yuko; INOUE, Katsuya; GOTO, Tsuneaki[1]
([1]ISSP, Univ. Tokyo)

[*J. Phys. Soc. Jpn.* **69**, 1008 (2000)]

We have synthesized novel organic polyradicals BIP-BNO and BIP-TENO, which crystallize to form spin systems with a double spin chain, where BIP-BNO and BIP-TENO denote 3,5’-bis(*N*-*tert*-butylaminoxyl)-3’,5’-dibromobiphenyl and 3,3’,5,5’-tetrakis(*N*-*tert*-butylaminoxyl)biphenyl, respectively. The crystals of BIP–BNO form a two-leg ladder of $S = 1/2$ with antiferromagnetic legs and rungs. The ground state of this material is singlet. The BIP–TENO molecule includes $S = 1/2$ spin pairs (dimers) in which the two spins are coupled ferromagnetically. The BIP-TENO crystals form a double spin chain consisting of dimers. All dimers interact antiferromagnetically with each other. This system can be regarded as an antiferromagnetic two-leg ladder when the dimer is taken as a unit. The ground state of this material is singlet and the existence of excitation gaps is suggested by the temperature dependence of the static magnetic susceptibility.

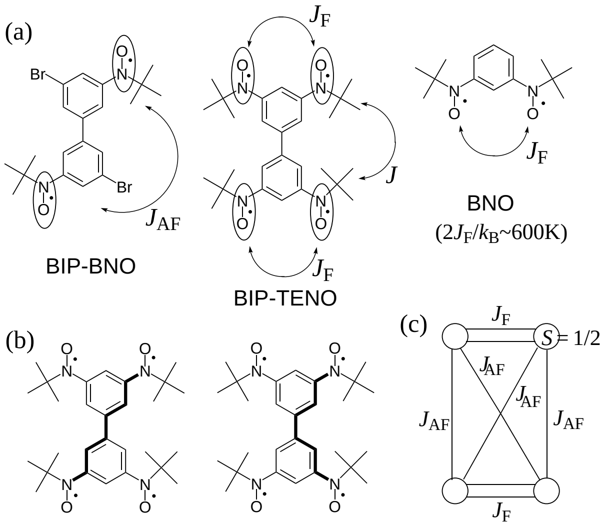

Figure 1. (a) Molecular structures of BIP-BNO, BIP-TENO and a related compound. Ellipses in BIP-BNO and BIP-TENO represent the spin-concentrated parts in a molecule. Each NO group corresponds to an S = 1/2 spin. (b) Path of the throughbond antiferromagnetic exchange interaction in BIP-TENO, which is indicated by bold lines. (c) Schematic diagram of the magnetic model of a BIP-TENO molecule. A circle, a double bond and a single bond represent an S = 1/2 spin, a ferromagnetic exchange coupling, and an antiferromagnetic exchange coupling, respectively.

V-F-4 Observation of Magnetization Plateau of 1/4 in a Novel Double Spin Chain of Ferromagnetic Dimmers Formed by an Organic Tetraradical

GOTO, Tsuneaki[1]; BARTASHEVICH, M. I.[1]; HOSOKOSHI, Yuko; KATOH, Keiichi[2]; INOUE, Katsuya
([1]ISSP, Univ. Tokyo; [2]GUAS)

[*Physica B* in press]

We have measured the susceptibility and low temperature magnetization curve of the novel organic tetraradical crystal BIP-TENO. The susceptibility data indicate that double spin chains of ferromagnetic dimmers are formed in the crystal and the spin system is regarded as an S = 1 antiferromagnetic two-leg ladder. The magnetization is nearly zero up to 10 T and the spin gap is closed at 11.6 T. Above 12 T, the magnetization increases and a plateau corresponding to a quarter of the saturation magnetization appears at 44.8 T.

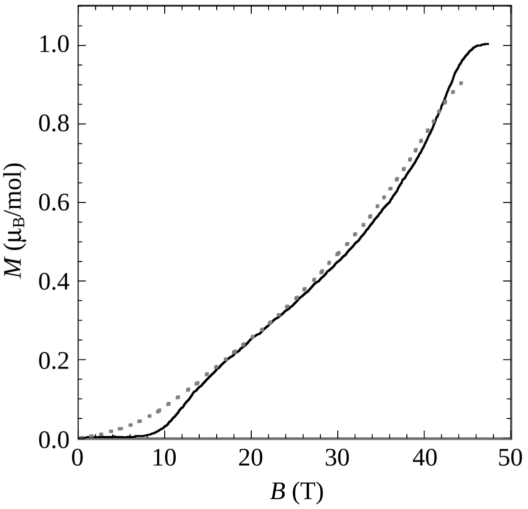

Figure 1. Magnetization curves of BIP–TENO for 1.7 K (solid) and 4.2 K (dotted) in pulsed high magnetic fields up to about 50 T.

V-G Pressure Effects on Molecular Magnetism

'Pressure' is a powerful tool to control the molecular packings and physical properties. The molecule-based materials with small densities are 'soft' and can be expected to exhibit large pressure effects. For the magnetic measurements with high-accuracy, we have developed a small high-pressure clamp cell made of non-magnetic Cu–Ti alloy which can be equipped to a Quantum Design SQUID magnetometer for the dc and ac magnetic measurements. The inner pressure of the clamp cell has been calibrated by the superconducting transition temperature of Pb. We have already discovered that some kind of structural change can be suppressed by pressurization. We are now studying the pressure effects on the molecule-based magnetic materials in wider range. In molecular materials, the spin density are delocalized and distributed in a molecule and the spin-density-distribution plays an important role in the exchange interactions. It is attractive to control the sign of the exchange coupling by pressurization. The pressure effects on the related compounds with similar crystal structures are studied.

V-G-1 Pressure Effect on Mn Complexes of Bisaminoxyl Radicals

HOSOKOSHI, Yuko; SUZUKI, Kentaro[1]; INOUE, Katsuya; IWAMURA, Hiizu[2]
([1]GUAS; [2]Kyushu Univ.)

[*Mol. Cryst. Liq. Cryst.* **334**, 511 (1999)]

The pressure effects on the magnetic properties of one-dimensional Mn(hfac)$_2$ complexes with 1,3-bis(*N*-*tert*-butylaminoxyl)benzene ($\mathbf{1}_H$) and 5-chloro-1,3-bis(*N*-*tert*-butylaminoxyl)benzene ($\mathbf{1}_{Cl}$) have been studied. These complexes have similar chain structures and, due to the weak interchain interactions, undergo three-dimensional magnetic phase transitions at low temperature. At ambient pressure, the former is a metamagnet with T_N = 5.4 K, and the latter is a ferrimagnet with T_C = 4.8 K. The opposite sign of the interchain interactions in these materials is attributed to the different way of packing of the chains. Application of the pressure less than 7 kbar to these materials mainly affects the interchain interactions. The high-temperature behaviour is almost independent of the pressure. In the metamagnetic compound of $[Mn(hfac)_2]\cdot\mathbf{1}_H$, enhancement of the antiferromagnetic interchain interactions by pressurization was observed. The transition temperature becomes higher and the critical field becomes larger with applying pressure. The closer spacing of each chains caused by pressurization, yields larger antiferromagnetic interchain interactions in this compound. On the other hand, the response to the pressure of the ferromagnetic compound of $[Mn(hfac)_2]\cdot\mathbf{1}_{Cl}$ is rather complicated. The transition temperature becomes higher and the antiferromagnetic interchain interactions are induced by pressurization. The interchain exchange coupling in this compound should be sensitive to the relative orientation of the chain structure. The decrease of the ferromagnetic contribution and/or the increase of the antiferromagnetic one in the interchain interactions is brought about by pressurization.

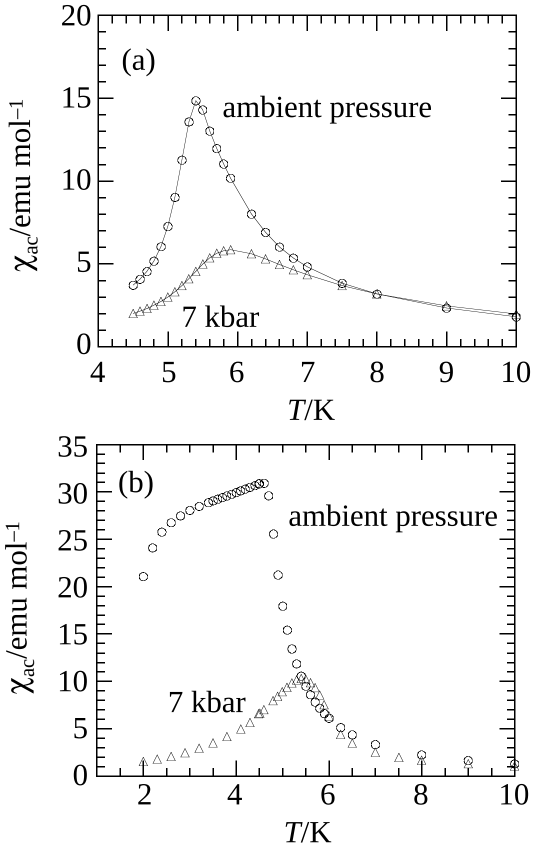

Figure 1. (a) Temperature dependence of the ac susceptibility of $[Mn(hfac)_2]\cdot\mathbf{1}_H$ at ambient pressure (○) and under 7 kbar (△). (b) Temperature dependence of the ac susceptibility of $[Mn(hfac)_2]\cdot\mathbf{1}_{Cl}$ at ambient pressure (○) and under 7 kbar (△).

V-G-2 Pressure Effect on $Cu(hfac)_2$ Complex with 5-Bromo-1,3-phenylenebis(*N-tert*-butyl-aminoxyl)—Suppression of the Structural Change under Pressure

HOSOKOSHI, Yuko; IWAHORI, Fumiyasu[1]; SUZUKI, Kentaro[1]; INOUE, Katsuya
([1]GUAS)

5-Bromo-1,3-phenylenebis(*N-tert*-butyl-aminoxyl) (**1**) forms a complex with $Cu(hfac)_2$ with the formula $[Cu(hfac)_2]_3\cdot\mathbf{1}_2$. The X-ray crystal structural analysis at room temperature revealed the discrete cluster formation of this unit. The temperature dependence of the susceptibility shows abrupt decrease at around 48 K with thermal hysteresis. The structural change at this temperature is suspected. We studied the magnetic properties under pressure and found that the anomaly at around 48 K disappears under 6 kbar. The susceptibility behaviour under 6 kbar is well understood based on the room-temperature crystal structure. Starting from the non-interacting 3 mol of $S = 1/2$ spin at room temperature, as temperature decreases, ferromagnetic exchange couplings within a cluster dominates the magnetism.

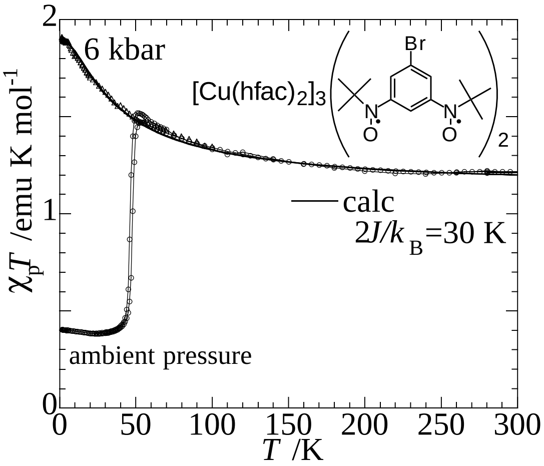

Figure 1. Temperature dependence of χ_pT of $[Cu(hfac)_2]_3\cdot\mathbf{1}_2$ at ambient pressure (○) and under pressure (△). Solid curve is the calclation for the ferromagnetic linear trimer model with $2J/k_B = 30$ K.

V-H Desorption Induced by Electronic Transitions at the Surface of Van der Waals Condensates

The electronic excitation on the surface of a van der Waals condensate may lead the desorption of neutral and charged molecules, either in the ground state or in excited ones. The phenomena discussed here are neither thermal desorption nor direct mechanical sputtering but processes through a transformation of an electronic excitation energy into a kinetic energy of a desorbing particle. Close investigation of this DIET (Desorption Induced by Electronic Transitions) phenomena will reveal the dynamical aspect of the electronic excitation and its relaxation process at the surface. In this research project, we have determined the absolute total desorption yield at the surface of solid Ne, Ar, and Kr and have investigated the desorption of the excimer, Ne_2*.

V-H-1 Absolute Measurement of Total Photo Desorption Yield of Solid Ne in Vacuum Ultraviolet Range

ARAKAWA, Ichiro[1]; ADACHI, Takashi[2]; HIRAYAMA, Takato[2]; SAKURAI, Makoto[3]
([1]IMS and Gakushuin Univ.; [2]Gakushuin Univ.; [3]Kobe Univ.)

[*Surf. Sci.* **451**, 136 (2000)]

Absolute yields of photo-induced desorption at the surface of solid Ne have been measured between 25 and 100 nm of wavelength of incident light. There are strong dependence of the total desorption yield of Ne both on the excitation energy and on the thickness of Ne films. On a thick film, the desorption yield is 1–2 atoms/photon by the bulk exciton excitation and 2–10 atoms/photon by the bulk ionization. The main component in the desorbed species is neutral Ne molecules in the ground state; the absolute yield of metastable desorption at the excitonic excitation is the order of 10^{-3} metastable/photon.1) The absolute yield of the order of unity for the total desorption by the bulk exciton excitation can quantitatively be understood by the following internal sputtering model. From optical absorption data, the number of excitons created per photon per layer is estimated at about 0.1. The kinetic energies of the particles desorbed through the cavity ejection mechanism is about 0.2 eV and those by the excimer dissociation one 1 eV. Because the cohesive energy of Ne is 0.019 eV, the desorbing paticle, which is originated from the 2nd or 3rd layer, can blow 10 or more neutral Ne atoms in the overlayer off. The product of these values results in an order of unity of absolute yield of the total desorption. By the surface exciton excitation, the yield is 0.1–0.3 atoms/photon, which value means that the desorption probability of the surface exciton is almost unity.

Reference

1) T. Hirayama, A. Hayama, T. Koike, T. Kuninobu, I. Arakawa, K. Mitsuke, M. Sakurai and E. V. Savchenko, *Surf. Sci.* **390**, 266 (1997).

V-H-2 Desorption of Excimers from the Surface of Solid Ne by Low Energy Electron or Photon Impact

HIRAYAMA, Takato[1]; HAYAMA, Akira[1]; ADACHI, Takashi[1]; ARAKAWA, Ichiro[2]; SAKURAI, Makoto[3]
([1]Gakushuin Univ.; [2]IMS and Gakushuin Univ.; [3]Kobe Univ.)

[*Phys. Rev. B* **63**, in press (2001)]

If solid Ne surface is irradiated by 20–200 eV electrons or by 55–75 nm synchrotron radiation, Ne_2* excimers in $^3\Sigma_u$ state are desorbed to form a luminescent ‘plume’ in front of the sample. The kinetic energy of the desorbed excimers was found to be 0.2 ± 0.1 eV, which indicates that the cavity ejection mechanism1) is valid for the excimer desorption. The decay with time of the plume emission is not of single exponential type, because the emission lifetime of the desorbed excimers, which is of the order of 10^{-6} s, depends on their vibrational level. Most of them are in the highest vibrational level since desorption takes place much faster than vibrational relaxation.

Reference

1) L. F. Chen, G. Q. Huang and K. S. Song, *Nucl. Instrum. Methods Phys. Res., Sect. B* **116**, 61 (1996).

V-I Bioinorganic Studies on Structures and Functions of Non-Heme Metalloenzymes Using Model Complexes

Metal-containing enzymes have been widely distributed in both plants and animals and have been related to metabolic processes such as hydroxylation, oxygen transport, oxidative catalysis, electron transfer, and so on. In this project the structures and functions for the metal complexes are studied as a model of several metallo-enzymes by some physico-chemical methods.

V-I-1 A Novel Diiron Complex as a Functional Model for Hemerythrin

ARII, Hidekazu[1]; NAGATOMO, Shigenori; KITAGAWA, Teizo; MIWA, Tomohiro[1]; JITSUKAWA, Koichiro[1]; EINAGA, Hisahiko[1]; MASUDA, Hideki[2]
([1]Nagoya Inst. Tech.; [2]Nagoya Inst. Tech. and IMS)

[*J. Inorg. Biochem.* in press (2000)]

Diiron(II) complexes with a novel dinucleating polypyridine ligand, *N*,*N*,*N'*,*N'*-tetrakis(6-pivalamido-2-pyridylmethyl)-1,3-diaminopropan-2-ol (HTPPDO), were synthesized as functional models of hemerythrin. Structural characterization of the complexes, $[Fe^{II}_2(Htppdo)(PhCOO)](ClO_4)_3$ (**1**), $[Fe^{II}_2(Htppdo)(p\text{-}Cl\text{-}PhCOO)](ClO_4)_3$ (**2**), $[Fe^{II}_2(Htppdo)(p\text{-}Cl\text{-}PhCOO)](BF_4)_3$ (**2'**) and $[Fe^{II}_2(tppdo)(p\text{-}Cl\text{-}PhCOO)](ClO_4)_2$ (**3**), were accomplished by electronic absorption and IR spectroscopic, electrochemical, and X-ray diffraction methods. The crystal structures of **1** and **2'** revealed that the two iron atoms are asymmetrically coordinated with HTPPDO and bridging benzoate. One of the iron centers (Fe(1)) has a seven-coordinate capped octahedral geometry comprised of an N_3O_4 donor set which includes the propanol oxygen of HTPPDO. The other iron center (Fe(2)) forms an octahedron with an N_3O_3 donor set and one vacant site. The two iron atoms are bridged by benzoate (**1**) or *p*-chlorobenzoate (**2**). On the other hand, both Fe atoms of complex **3** are both symmetrically coordinated with N_3O_4 donors and two bridging ligands, benzoate and the propanolate of TPPDO. Reactions of these complexes with dioxygen were followed by electronic absorption, resonance Raman and ESR spectroscopies. Reversible dioxygen-binding was demonstrated by observation of an intense LMCT band for O_2^{2-} to Fe(III) at 610 (**1**) and 606 nm (**2**) upon exposure of dioxygen to acetone solutions of **1** and **2** prepared under an anaerobic conditions at –50 °C. The resonance Raman spectra of the dioxygen adduct of **1** exhibited two peaks assignable to the ν(O–O) stretching mode at 873 and 887 cm^{-1}, which shifted to 825 and 839 cm^{-1} upon binding of $^{18}O_2$. ESR spectra of all dioxygen adducts were silent. These findings suggest that dioxygen coordinates to the diiron atoms as a peroxo anion in a μ-1,2 mode. Complex **3** exhibited irreversible dioxygen binding. These results indicate that the reversible binding of dioxygen is governed by the hydrophobicity of the dioxygen-binding environment rather than the iron redox potentials.

V-I-2 Reactivity of Hydroperoxide Bound to a Mononuclear Non-Heme Iron Site

WADA, Akira[1]; OGO, Seiji; NAGATOMO, Shigenori; KITAGAWA, Teizo; WATANABE, Yoshihito; JITSUKAWA, Koichiro[1]; MASUDA, Hideki[2]
([1]Nagoya Inst. Tech.; [2]Nagoya Inst. Tech. and IMS)

The first isolation and spectroscopic characterization of the high-spin mononuclear iron(III) complex with hydroperoxide in an end-on mode, $[Fe(bppa)(OOH)]^{2+}$, and the stoichiometric oxidation of substrates by the mononuclear iron-oxo intermediate produced by its decomposition have been described. The purple species (**2**) obtained from reaction of $[Fe(bppa)(HCOO)](ClO_4)_2$ with H_2O_2 in acetone solution at -50 °C gave characteristic UV-vis (λ_{max} = 568 nm, ε = 1200 $M^{-1}cm^{-1}$), ESR (g = 7.54, 5.78 and 4.25, S = 5/2), and ESI mass spectra (m/z = 288.5 corresponding to the ion, $[Fe(bppa)(OOH)]^{2+}$). The resonance Raman spectrum of **2** in d_6-acetone revealed two intense bands at 621 and 830 cm^{-1}, in which the former band shifted to 599 cm^{-1} when reacted with ^{18}O-labeled H_2O_2 and the latter band showed a small isotope shift to 813 and 826 cm^{-1} upon reaction with of $H_2{}^{18}O_2$ and D_2O_2, respectively. Reactions of the isolated $(bppa)Fe^{III}\text{-}OOH$ (**2**) with various substrates (single turnover oxidations) revealed that the iron-oxo intermediate generated by decomposion of complex **2** is a nucleophilic intermediate formulated as $[(bppa)Fe^{III}\text{–}O^{\bullet}]$.

V-J Synthesis and Physical Properties of Novel Molecular Metals

Development of organic materials which exhibit interesting electrical properties such as metallic conductivity and superconductivity has received considerable attention. A bis-fused TTF, 2,5-bis(1,3-dithiol-2-ylidene)-1,3,4,6-tetrathiapentalene (TTP) is a promising π-electron framework for preparation of stable metals down to low temperatures, because it has a ladder-like array of sulfur atoms indispensable for constructing two-dimensional network of the donors. In fact, we have found that the unsubstituted TTP has a strong tendency to afford highly conducting radical cation salts retaining metallic conductivity down to $\leq$ 1.2 K regardless of shape and size of counter anions. In the present study, we have developed several organic metals by means of comprehensive modification of TTP, namely i) introduction of substituents, ii) exchange of sulfur atoms in the TTP framework with selenium, iii) synthesis of TTP analogs possessing non-TTF donor unit.

V-J-1 Preparation, Structures and Physical Properties of Selenium Analogues of DTEDT as Promising Donors for Organic Metals

FUJIWARA, Hideki[1,2]; MISAKI, Yohji[1,2]; YAMABE, Tokio[1]; MORI, Takehiko[2,3]; MORI, Hatsumi[4]; TANAKA, Shoji[4]
([1]Kyoto Univ.; [2]IMS; [3]Tokyo Inst. Tech.; [4]ISTEC)

[*J. Mater. Chem.* **10**, 1565 (2000)]

Three selenium analogues of DTEDT [2-(1,3-dithiol-2-ylidene)-5-(2-ethanediylidene-1,3-dithiole)-1,3,4,6-tetrathiapentalene] have been synthesized. They showed four pairs of single-electron redox waves. The E_1 values are a little higher by 0.02–0.05 V than that of DTEDT. On the other hand, the E_2–E_1 values are almost equal to that of DTEDT. TCNQ complex and cation radical salts of them show fairly high electrical conductivities and several salts exhibit metallic conductivities. Especially the ReO_4^- and $Au(CN)_2^-$ salts of DTEDS and the SbF_6^-, TaF_6^- and I_3^- salts of DSEDS exhibited stable metallic behaviour down to 1.5–4.2 K. An X-ray crystal structure analysis of the metallic salt $(DSEDS)_3TaF_6$ reveals that this salt has two-dimensional β-type packing motif of donor molecules similar to the superconducting $(DTEDT)_3Au(CN)_2$. The calculated Fermi surface of $(DSEDS)_3TaF_6$ is a two-dimensional closed ellipsoid.

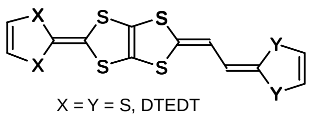

X = Y = S, DTEDT
X = S, Y = Se, DTEDS
X = Se, Y = S, DSEDT
X = Y = Se, DSEDS

(a)

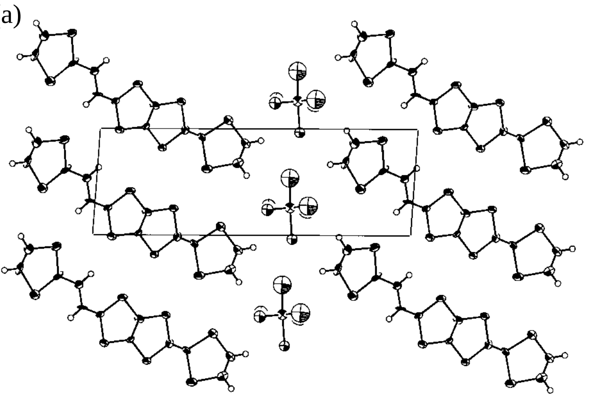

(b)

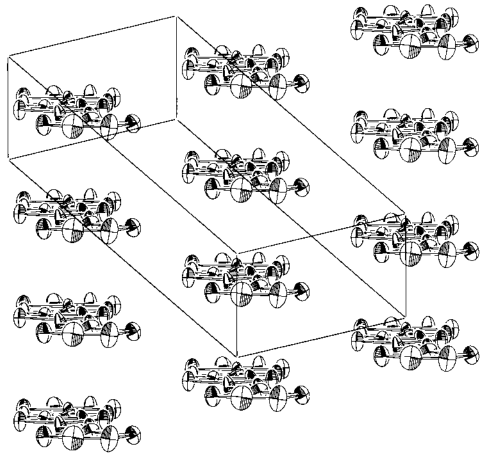

Figure 1. Crystal structures of $(DSEDS)_3TaF_6$ viewed (a) along the *c*-axis and (b) along the molecular long axis.

V-J-2 Preparation and Properties of Gold Complexes with TTF Dithiolato Ligands

MISAKI, Yohji[1,2,3]; TANI, Yoshihiro[1]; TANIGUCHI, Masateru[1]; MAITANI, Tatsuyuki; TANAKA, Kazuyoshi; BECHGAARD, Klaus[3]
([1]Kyoto Univ.; [2]IMS; [3]Risø National Lab.)

[*Mol. Cryst. Liq. Cryst.* **343**, 59 (2000)]

Several gold(III) complexes with TTF dithiolato ligands have been prepared as the tetrahexylammonium salts. The cyclic voltammograms in DMF showed two or three pairs of redox waves. X-Ray structure analysis of $Ph_4P{\cdot}Au(eodt)_2{\cdot}(DMF)_2$ reveals that the $Au(eodt)_2$ anion takes a significantly folded chair conformation. Charge-transfer salts of $Au(dt)_2$ derivatives with TCNQ showed high conductivity (σ_{rt} = 10^0–10^1 S cm^{-1} on a compressed pellet).

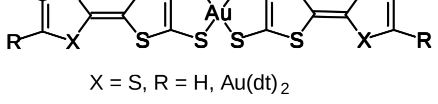

X = S, R = H, $Au(dt)_2$
X = S, R = SMe, $Au(tmdt)_2$
X = S, R = SEt, $Au(tedt)_2$
X = S, 2R = $-(CH_2)_4-$, $Au(chdt)_2$
X = S, 2R = $-O(CH_2)_2O-$, $Au(eodt)_2$
X = Se, R = H, $Au(ds)_2$

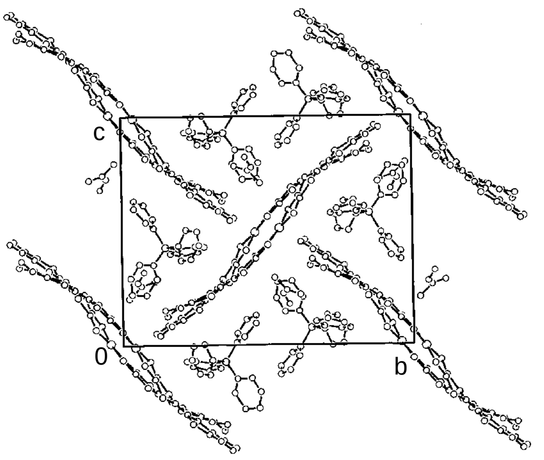

Figure 1. Crystal structure of $Ph_4P\cdot Au(eodt)_2\cdot (DMF)_2$ viewed onto the *bc* plane.

V-J-3 New TTP Donors Containing Chalcogenopyran-4-ylidene: Preparation, Structures, and Electrical Properties

TAKAHASHI, Kazuyuki[1]; NAKAYASHIKI, Takashi[1]; MISAKI, Yohji[1,2]; TANAKA, Kazuyoshi[1]
([1]Kyoto Univ.; [2]IMS)

Several selenium analogues of TM-PDT-TTP (2-[4,5-bis(methylthio)-1,3-dithiol-2-ylidene]-5-(pyran-4-ylidene)-1,3,4,6-tetrathiapentalene), SM-PDT, SM-TPST, SM-SPDT, and TM-SPDT have been prepared. Among them, SM-PDT affords relatively high conducting 1:1 radical cation salt, $(SM\text{-}PDT)AsF_6\cdot H_2O$ (σ_{rt} = 8.3 S cm^{-1}, E_a = 0.045 eV). X-Ray structure analysis of $(SM\text{-}PDT)AsF_6\cdot H_2O$ revealed that the side-by-side interactions are inhibited owing to existence of the anions on the side of the donor columns. Instead, the donors form two-dimensional sheets thanks to significant interaction along the donor long axis as well as stacking structure (Figure 1).

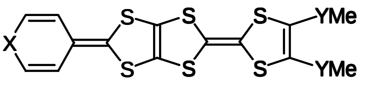

X = O, Y = S, TM-PDT
X = O, Y = Se, SM-PDT
X = S, Y = Se, SM-TPDT
X = Se, Y = Se, SM-SPDT
X = Se, Y = S, TM-SPDT

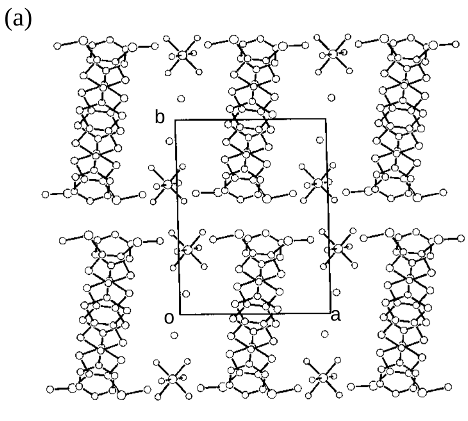

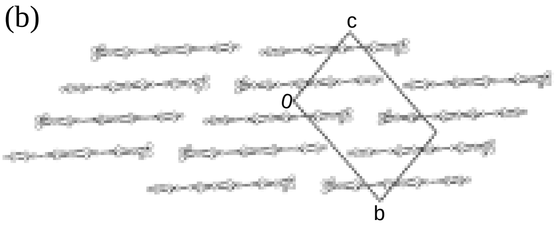

Figure 1. Donor sheet structure of $(SM\text{-}PDT)AsF_6\cdot H_2O$.

V-J-4 Structures and Properties of CHEO-TTP Salts

TANIGUCHI, Masateru[1]; MIURA, Takeshi[1]; MISAKI, Yohji[1,2]; TANAKA, Kazuyoshi[1]; YAMABE, Tokio[1]; MORI, Takehiko[2,3]
([1]Kyoto Univ.; [2]IMS; [3]Tokyo Inst. Tech.)

Radical cation salts of CHEO-TTP, where CHEO-TTP is 2-(4,5-cyclohexeno-1,3-dithiol-2-ylidene)-5-(4,5-ethylenedioxy-1,3-dithiol-2-ylidene)-1,3,4,6-tetrathiapentalene showed metallic temperature dependence down to liquid helium temperature. An X-ray crystal structure analysis of $CHEO\text{-}TTP(ReO_4)_{0.35}$ reveals that the arrangement of the donors is the so-called κ-type. The band structure calculated based on a tight-binding approximation suggests the present salt has a two-dimensional Fermi surface similar to those of the superconducting κ-type salts.

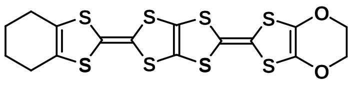

CHEO-TTP

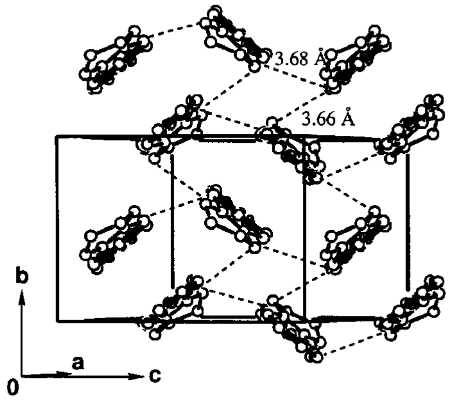

Figure 1. Donor sheet structure of $CHEO\text{-}TTP(ReO_4)_{0.35}$.

V-J-5 Structures and Physical Properties of $(CHTM\text{-}TTP)_2TCNQ$

TANIGUCHI, Masateru[1]; MISAKI, Yohji[1,2]; TANAKA, Kazuyoshi[1]; MORI, Takehiko[2,3]; NAKAMURA, Toshikazu
([1]Kyoto Univ.; [2]IMS; [3]Tokyo Inst. Tech.)

X-Ray structure analysis of the title compound revealed that the donors form a two-dimensional conducting sheets of the so-called β-type, while no significant interaction was observed in the TCNQ sheets. The frequency of CN stretching obtained by IR spectroscopy suggested the degree of charge-transfer in

TCNQ is about –1. A tight binding band calculation indicates the present complex has a quasi one-dimensional Fermi surface closed to the stacking direction. It exhibited metal-like temperature dependence of resistivity down to T_{MI} = 30 K though the resisitvity increased one around 220 K.

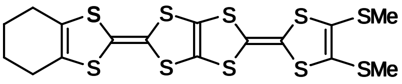

CHTM-TTP

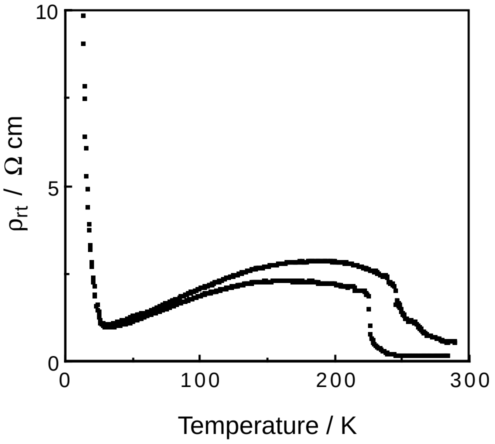

Figure 1. Conducting behaviour of (CHTM-TTP)$_2$TCNQ.

V-K Fast Bimolecular Reaction Kinetics in Solution

Since April 2000, we started a new research project for obtaining microscopic pictures of chemical reactions in a solution phase. For this purpose, we construct a new time-resolved spectrometer that can trace reaction kinetics in solution with a time resolution of a few hundreds of femtoseconds. In particular, we try to detect time dependent transient absorption in the near-infrared region accompanying photoexcitation of reactant molecules and following photochemical reactions. A mode-locked Ti:sapphire laser system modified by Prof. Taira’s Group, Laser Research Center for Molecular Science, will be used for this study.

V-K-1 Ultrafast Bimolecular Reaction Kinetics between S_1 *trans*-Stilbene and Carbon Tetrachloride Studied by Sub-Picosecond Time-Resolved Visible Absorption Spectroscopy

IWATA, Koichi[1,2]; HAMAGUCHI, Hiro-o[1]
([1]Univ. Tokyo; [2]IMS)

[*Chem. Lett.* 456 (2000)]

Ultrafast bimolecular reaction kinetics between S_1 *trans*-stilbene and carbon tetrachloride is monitored by sub-picosecond time-resolved visible absorption spectroscopy. After the photoexcitation at 270 nm, the S_n–S_1 transition of *trans*-stilbene observed at 580 nm is quenched in a few picoseconds due to a bimolecular photochemical reaction between *trans*-stilbene and carbon tetrachloride. The observed reaction kinetics is well explained by assuming a time dependent bimolecular rate constant derived either from Smoluchowski’s theory or from Collins-Kimball’s theory of diffusion-controlled reactions. It is not obvious if diffusion is a suitable concept for describing a translational motion of molecules in a time period of a few picoseconds. The model of diffusion should be used for transportation phenomena, such as heat dissipation or molecular motion, in a macroscopic system. However, the experimental result suggests that the molecular motion in solution for a few picosecond time period is well described as a diffusion process for this molecular system.

V-L Development of Model Core Potentials and Post Hartree-Fock Calculations to Atoms and Molecules

We have developed various types of model core potentials for various elements and applied the MCPs to investigate the electronic structures of atoms, molecules, and clusters at levels of post Hartree-Fock calculations. We also investigaed the electronic and vibrational structures of molecules using basis functions for all electrons.

V-L-1 A Theoretical Study on the Ionization of CO_2 and CS_2 with Analysis of the Vibrational Structure of the Photoelectron Spectra

TAKESHITA, Kouichi[1]; SHIDA, Norihiro[2]; MIYOSHI, Eisaku
([1]Tokyo Univ. Agric.; [2]Nagoya Inst. Tech.)

[*J. Chem. Phys.* **112**, 10838 (2000)]

We have studied the vibrational eigenfunctions, the Frank-Condon factors (FCFs), and the theoretical intensity curves of the four ionic states ($^2\Pi_g$, $^2\Pi_u$, $^2\Sigma_u{}^+$, and $^2\Sigma_g{}^+$) of CO_2 and CS_2 by explicit vibrational calculations using the global region of the potential energy (PE) surface at the MRSDCI level.

The theoretical intensity curves reproduce well the PE spectra. An assignment of the vibrational structures agrees in most cases with that obtained by Turner *et al.*

For the first ionic state ($^2\Pi_g$) of CO_2, the vibrational excitations of the antisymmetric stretching mode should be observed. This situation is connected with the fact that the difference of the vibrational frequencies of the antisymmetric stretching mode between the final and initial states is large. The difference between the two is 1063 cm^{-1}. The FCFs of the (0 0 2) and (1 0 2) transitions are 0.013 and 0.005, respectively. For the first ionic state ($^2\Pi_g$) of CS_2, the difference of the two is 220 cm^{-1}, which is a fifth of that for CO_2. The FCF of the (0 0 2) transition is 0.002.

The spectra of the second ionic states ($^2\Pi_u$) of CO_2 and CS_2 have broad features compared with the other states. This is attributed to the large change (~0.06 Å) in the bond length upon ionization. The change of the $^2\Pi_u$ state is more than three times as large as that of the other states.

V-L-2 A Theoretical Study on the Ionization of OCS with Analysis of the Vibrational Structure of the Photoelectron Spectrum

TAKESHITA, Kouichi[1]; SHIDA, Norihiro[2]; MIYOSHI, Eisaku
([1]Tokyo Univ. Agri.; [2]Nagoya Inst. Tech.)

[*Theor. Chem. Acc.* submitted]

We have studied the vibrational eigenfunctions, the Frank-Condon factors (FCFs), and the theoretical intensity curves of the four ionic states ($1^2\Pi$, $2^2\Pi$, $1^2\Sigma^+$, and $2^2\Sigma^+$) of OCS by explicit vibrational calculations using the global region of the potential energy (PE) surface at the MRSDCI level.

The theoretical intensity curves reproduce well the PE spectrum except for the spin-orbit splitting. The present calculation supports the assignment of the vibrational structures obtained by Turner *et al.* Delwiche *et al.* have reported the more resolved PE spectrum. An assignment of the vibrational structures is almost consistent with their assignment.

The present calculation proposes the following additional assignment: For the fourth peak of the first ionic state, the (3 0) transition also contributes to intensity in addition to the (0 1) transition. The weak peak at 18.6 eV of the fourth ionic state should be assigned to the (1 2) transition.

V-L-3 Configuration Interaction Study of Differential Correlation Energies in Ca^+, Ca and Ca^-

OSANAI, You[1]; NORO, Takeshi[2]; MIYOSHI, Eisaku
([1]Aomori Univ.; [2]Hokkaido Univ.)

[*Phys. Rev. A* **62**, in press (2000)]

Configuration interaction (CI) calculations have been carried out for Ca^+ (4s ^2S, 3d ^2D and 4p $^2P^o$), Ca ($4s^2$ ^1S and 3d4s ^1D) and Ca^- ($4s^24p$ $^2P^o$) using very large Slate-type orbitals. The effect of Ar-like core was included by allowing the excitation from the most important subshells of the core, 3s and 3p, explicitly. A series of multi-reference single and double excitation CI calculations was performed adding important configurations representing valence correlation to the reference space, and convergence of CI energies and wavefunctions was investigated. Valence correlation can be described adequately only when the reference space is expanded so largely that valence correlation is almost completely described by reference functions alone. The relativistic effects were estimated by carrying out Dirac-Fock calculations. The present calculations gave the ionization potentials to 4s ^2S, 3d ^2D and 4p $^2P^o$ to be 6.079, 7.819 and 9.179 eV, respectively, and the excitation energy to 3d4s ^1D to be 2.805 eV. All these calculated values are in good agreement with the observed values. The electron affinity was obtained to be 17.7 meV, which is in excellent agreement with the recent observed values, 17.5 ~ 21.5 meV.

V-L-4 Spin-Orbit Configuration Interaction Calculations of Low-Lying Electronic States of NaCl Using Model Core Potential

MIYOSHI, Eisaku; SEIJO, Luis; SAKAI, Yoshiko[1]
([1]Kyushu Univ.)

We performed spin-orbit CI calculations for the low-lying $\Omega = 0^+$ states of the NaI molecule in the framework of the model core potentail (MCP) method.

For the I atom, we used scalar relativistic dsp-MCP and (8s/7p/6d) basis set augmented with one diffuse s- and p-type GTFs and two d- and f-type polarization GTFs, resulting in (6111/5111/5111/11). For the Na atom, we used all-electron (533/5) augmented with two p- and d-type polarization GTFs, resulting in (521111/4111/11). The spin-orbit term was calculated in the follwing form:

$$V^{mcp}_{SO,nl}(r) = \lambda \sum_i \frac{B_i \exp\left(-\beta_i r^2\right)}{r^2}$$

where λ is a scaling factor.

The potential energy curve of the $A^1\Sigma^+$ state calculated at spin-free scalar relativistic treatment (quasi-relativistic calculation including only mass-velocity and Dawin terms) is almost the same as those given by previous MO calculations but the potential energy curve of the first excited $A0^+$ state calculated at spin-orbit CI treatment is almost the same as those given from the data of previous experiments. The first excited $A0^+$ state has a weight (80%) of the covalent $^3\Pi$ state and 20% of the covalent $A^1\Sigma^+$ state around the ground state equilibrium distance. Thus, the state can be a dipole-allowed transition state with a large transition probability from the ionic ground $X^1\Sigma^+$ state.

V-M Theoretical Study of the Electronic Structures of Weakly Bound Molecules

The electronic structures of weakly bound molecules such as van der Waals molecules are investigated by using sophisticated methods for electronic states, *i.e.*, multi-reference single and double excitation configuration interaction (MRSDCI) and multi-reference coupled pair approximation (MRCPA) calculations.

V-M-1 *Ab initio* Molecular Orbital Study of Fe(CO)$_n$ (n = 1, 2, and 3)

HONDA, Hiroaki[1]; NORO, Takeshi[1]; MIYOSHI, Eisaku
([1]Hokkaido Univ.)

[*Theor. Chem. Acc.* **104**, 140 (2000)]

Various unsaturated iron carbonyl complexes Fe(CO)$_n$ (n = 1 to 4) have been produced by the UV photolysis of iron pentacarbonyl Fe(CO)$_5$. Among them the spectroscopic studies of the FeCO radical has been extensively performed from both experimental and theoretical points of view and there have been a few experimental spectroscopic constants of Fe(CO)$_2$ and Fe(CO)$_3$.

Although there have been published several theoretical studies for Fe(CO)$_2$ and Fe(CO)$_3$, there are few comprehensive studies for the change of bonding nature in the Fe(CO)$_n$ (n = 1 to 3) radicals. In this study we have carried out MCSCF calculations for the Fe(CO)$_n$ (n = 1 to 3) to investigate the nature of bonding respect to change in the number of CO ligands. The calculated bond lengths of R(Fe–C) are reasonably in agreement with experimental values and more sophisticated theoretical results. From the Mulliken population analysis, the traditional donation and back donation mechanism is valid for FeCO through Fe(CO)$_3$.

V-M-2 *Ab initio* CASSCF and MRSDCI Calculations of the $(C_6H_6)_3^+$ Radical

MIYOSHI, Eisaku; GHOSH, Tapas Kumar

[*Chem. Phys. Lett.* **323**, 434 (2000)]

Ab initio complete active space self-consistent-field (CASSCF), single-reference singly and doubly excited configuration interaction (SRSDCI), and multi-reference SDCI (MRSDCI) calculations were performed for the benzene trimer cation radical, $(C_6H_6)_3^+$, in the ground state. We obtained the equilibrium geometry of the D_{6h} sandwich structure and found that the global minimum of the cation is at the distorted C_{2v} sandwich structures. This minimum is 0.032 eV lower than that of the D_{6h} sandwich structure. The dissociation energy (D_e) relative to $(C_6H_6)_2^+$ + C_6H_6 was calculated to be 0.43 eV, in comparison to the experimental value (D_0) of 0.34 ± 0.02 eV. Our calculations suggest that the bands observed by Nishi and co-workers at 1.02 and 1.29 eV can both be assigned to the split components of the $^2E_{1u}$ state, which are charge resonance states. This is also the case for the benzene dimer cation radical. In the ground state of the trimer cation radical, almost all the charge is localized at the central benzene ring, which has a gross charge of +0.9. This observation contrasts with speculations by experimentalists that the charge is localized in the dimer core or delocalized over all three benzene rings.

V-M-3 Molecular Orbital Study on OH Stretching Frequency of Phenol Dimer and its Cation

GHOSH, Tapas Kumar; MIYOSHI, Eisaku

[*Theor. Chem. Acc.* **105**, in press(2000)]

Ab initio calculations were performed to investigate the structure and bonding of the phenol dimer and its cation, especially, the OH stretching frequencies. Some stable structures of the phenol dimer and its cation were obtained at the Hartree-Fock level and were found in agreement with predictions based on spectroscopic investigations. In these dimers the phenol moieties are bound by a single OH··O hydrogen bond. The hydrogen bond is much stronger in the dimer cation than in the neutral dimer. The calculated binding energy of the phenol dimer in the most stable structure was 6.5 ~ 9.9 kcal/mol at various levels of calculation compared with the experimental value of ≥ 5 kcal/mol. The binding energy of the phenol dimer cation is more than three times (24.1 ~ 30.6 kcal/mol) as large as that of the neutral dimer. For the phenol dimer the OH stretching frequency of the proton accepting phenol (PAP) is 3652 cm^{-1} and that of the proton donating phenol (PDP) is 3516 cm^{-1}; these are in agreement with observed values of 3654 cm^{-1} and 3530 cm^{-1}, respectively. For the phenol dimer cation the OH stretching frequency of the PAP is 3616 ~ 3618 cm^{-1} in comparison with an observed value of 3620 ± 3 cm^{-1}. That of the PDP in the dimer cation is calculated to be 2434 ~ 2447 cm^{-1}, which is 1210 ~ 1223 cm^{-1} smaller than that of the bare phenol. The large reduction of the OH stretching frequency of the PDP in the phenol dimer cation is attributed to the formation of a stronger hydrogen bond in the cation than in the neutral dimer.

V-N Theory for Quantum Liquids and Molecular Dynamics Study Using Potentials by *ab initio* Molecular Orbital Calculations

We derived generalized Ornstein-Zernike equations for quantum liquids. The set of equations can be applicable to homogeneous and isotropic Bose and Fermi liquids such as ^{3}He, ^{4}He, and electron liquids at arbitrary temperature. Using potentials obtained by ab initio molecular orbital calculations, molecular dynamics calculations were also performed to investigate physical properties of liquid mercury.

V-N-1 An Integral Equation Theory for Quantum Liquids: Finite-Temperature Kohn-Sham Debsity-Functional Formulation

SUMI, Tomonari; SATO, Hirofumi; HIRATA, Fumio; MIYOSHI, Eisaku

[*Phys. Rev. E* submitted]

We derived a generalized Ornstein-Zernike equation for quantum liquids, where the uncertainty in particle position is considered by using a self-correlation function for an ideal quantum liquid. To determine a self-consistent solution of the finite-temperature Kohn-Sham equation introduced by Chihara [*Prog. Theor. Phys.* **50**, 1156 (1973)] combined with the generalized Ornstein-Zernike equation for quantum liquids, we present two types of closure relation. One is obtained by extending Percus' method for quantum liquids, and the other is derived from the nonlinear Debye-H_ckel approximation. These sets of equations can be used to determine the pair correlation function and the direct correlation function for homogeneous and isotropic Bose and Fermi liquids.

V-N-2 Structure Change of Supercritical Mercury

SUMI, Tomonari; MIYOSHI, Eisaku

It has been well known that density fluctuations and correlation lengths which are related to the long-range structure of liquids have maxima in the supercritical region. Morita *et al.* found by using small-angle X-ray scattering experiments that the maxima for supercritical water, CO_2, and CF_3H are in a little lower density region than the critial isochore.$^{1)}$ They also estimated the density fluctuations and correlation lengths of Hg by using the equations of state and showed that the maxima are in the lower density region from the critical isochore and the deviations become larger with increasing temperature.

We have performed molecular-dynamics (MD) calculations for liquid mercury in the regions including the metal-nonmetal transition region under pair-potential approximation using the potential energy curve of the dimeric Hg, and showed that the pair-potential approximation gives a good qualitative description of the metallic interatomic force for liquid mercury and MD calculations using this approximation demonstrate the characteristic change of force fields between liqiud metal and liquid semiconductor.$^{2)}$ In the present study, we performed MD calculations for superdritical mercury under fixed pressures and discussed the relationship between fluctuations of the long-range structure and the change of the local structure.

The density dependence of the first peak of the pair distribution function were examined for supercritical mercury under a fixed pressure, showing that the peak shifts to longer distance with decreasing density, while the peak height has minimum at a density. This change is due to a crossover from shorter distance between the nearest neighboring atoms in liquid phase to longer distance in gas phase. It can be easily considered that the fluctuations of local structure become large near the crossover region.

References

1) T. Morita *et al.*, *J. Chem. Phys.* **112**, 4203 (2000).
2) T. Sumi, E. Miyoshi and K. Tanaka, *Phys. Rev. B* **59**, 6153 (1999).

V-O Determination of Structures of Neutral Clusters

The relationship between the structure and dynamics in floppy systems is a subject that has focused much attention recently. Specifically the "geared interconversion" of hydrogen bonded dimers such as $(HCl)_2$, $(DCl)_2$, and $(HF)_2$ have been studied extensively both experimentally and theoretically. Most of the experimental studies focused on the spectroscopy of these species, from which the tunneling splitting could be extracted. We applied a hexapole field to extract the dipole moment of $(HCl)_2$ and we find that interconversion'' of hydrogen bonded dimers can be directly observed by the hexapole field method. Secondly, the metal-ligand cluster beam serves as a model system for studying metal-ligand interaction, however little is known about interaction between Al and simple molecule as isolated system in the gas phase. We demonstrate again how successfully the hexapole method can be applied to newly synthesized complexes of Al–CH_3CN and Al–NH_3.

V-O-1 Focusing of DCl and HCl Dimers by an Electrostatic Hexapole Field—The Role of the Tunneling Motion

IMURA, Kohei[1]; KASAI, Toshio[2]; OHOYAMA, Hiroshi[1]; NAAMAN, Ron[3]
([1]Osaka Univ.; [2]IMS and Osaka Univ.; [3]Weizmann Inst. Sci.)

[*J. Chem. Phys.* **110**, 355 (1999)]

The focusing of HCl and DCl dimers was observed using a 2-m-long electrostatic hexapole field. The results indicate the existence of two types of species. The first is the homodimers, either the $H^{35}Cl{\cdot}H^{35}Cl$ or the $D^{35}Cl{\cdot}D^{35}Cl$, for which the data indicate a fast tunneling motion. The second is the heterodimers, $H^{35}Cl{\cdot}H^{37}Cl$ or $D^{35}Cl{\cdot}D^{37}Cl$, that do not show evidence for significant tunneling motion on the time scale of the experiment. In the case of HCl dimers, even at relatively high fields, only one species could be focused, the heterodimer. The electric dipole moments for both $(DCl)_2$ isotopomers were determined to be 1.5 ± 0.2 D, which is the same value as observed for $(HCl)_2$.

V-O-2 Tunneling Motion in $(HCl)_2$ Hydrogen-Bonded Dimer Probed by Electrostatic Hexapole and Doppler-Selected TOF Measurement for the Internal Energy Distribution of [ClHCl]

IMURA, Kohei[1]; OHOYAMA, Hiroshi[1]; NAAMAN, Ron[2]; CHE D.-C.[3]; HASHINOKUCHI, Masahiro[3]; KASAI, Toshio[3]
([1]Osaka Univ.; [2]Weizmann Inst. Sci.; [3]IMS and Osaka Univ.)

[*J. Mol. Struct.* **552**, 137 (2000)]

The tunneling motion in $(HCl)_2$ hydrogen bonded dimer and its deuterate was probed by a 2-m long electrostatic hexapole field. The focusing curves of the dimers confirmed existence of homo and hetero dimers in the cluster beam. The homodimer, either $H^{35}Cl{\cdot}H^{35}Cl$ or $H^{37}Cl{\cdot}H^{37}Cl$, undergoes fast tunneling motion for the two hydrogen atoms in the dimer. The heterodimer, namely $H^{35}Cl{\cdot}H^{37}Cl$ on the other hand, does not show such fast tunneling motion on the time scale of experiment. The observed ratio of homo to hetero dimer was estimated to be 20 ± 10, and this value differs largely from the natural abundance for chlorine isotope. An experimental scheme to discern homo and hetero dimers is proposed here. By looking at fragments in $(HCl)_2$ dimer photodissociaiton using a Doppler-selected time-of-flight (TOF) technique, internal energy distribution of [ClHCl] fragment was measured in 121.6-nm photodissociation. The TOF spectrum consists of fast and slow velocity components for dissociated H atoms. It is found that the slow H component arises from the hydrogen escapes after many collisions. The fast H component arises from direct H escape without any collision, thus this component reflects internal and/or electronic state of counter part fragment, *i.e.* [ClHCl]. Vibrational structure of [ClHCl] was observed for the fast H component of the TOF spectrum.

V-P Reaction Dynamics in the Gas Phase and on Surface

The reactions of metastable rare gas atoms with small molecules have provided a long-standing interest, because of the variety of possible involved reaction channels. These include electronic energy transfer, molecular dissociation, excimer formation, Penning ionization, etc. Among them, Penning ionization has been widely studied in recent years. It has been suggested that anisotropy effects influence Penning ionization. We explore the stereodynamical aspect of this reaction using the oriented molecular beam of CH_3Cl.

Surface reactions of hydrogen with atomic and molecular adsorbates on metal and semiconductor surfaces have been paid much attention because of the fundamental interest in the mechanism and dynamics of these reactions. Especially, abstraction of chemisorbed H(D) atoms by the gas-phase H(D) atoms have been extensively studied theoretically and experimentally because of its simplicity and its important roles in the catalytic reactions. We directly identify the desorbed molecules during the reaction and discuss a possible model of H-D exchange reaction.

V-P-1 Evidence for Steric Effect in Methyl Chloride Ionization by Metastable Argon Atoms

OHOYAMA, Hiroshi[1]; KAWAGUCHI, Hiroshi[1]; YAMATO, Masanori[1]; KASAI, Toshio[2]; BRUNETTI, Brunetto G.[3]; VECCHIOCATTIVI, Franco[3]
([1]Osaka Univ.; [2]IMS and Osaka Univ.; [3]Univ. Perugia)

[*Chem. Phys. Lett.* **313**, 484 (1999)]

The orientation dependence of methyl chloride ionization by collision with metastable argon atoms at an average collision energy of 0.09 eV has been investigated, using an electric hexapole field selector followed by an orienting field. The steric opacity function of the process has been determined. The highest reactivity has been found for approaches of the metastable atom towards the Cl-end of the molecule, while the lowest corresponds to the opposite approaches close to the CH_3-end. The stereo-selectivity is discussed in terms of spatial distribution of the highest occupied molecular orbital of CH_3Cl, mainly localized on the chlorine atom.

V-P-2 Direct Observation of Steric Effect in Penning Ionization Reaction of Ar* + $CHCl_3 \rightarrow CHCl_2^+ + Cl + e^- + Ar$

YAMATO, Masanori[1]; OKADA, Seiki[1]; WU, Victor Wei-Keh[1]; OHOYAMA, Hiroshi[1]; KASAI, Toshio[2]
([1]Osaka Univ.; [2]IMS and Osaka Univ.)

[*J. Chem. Phys.* **113**, 6673 (2000)]

Steric effect in the Penning ionization reaction of Ar* ($^3P_{2,0}$) + $CHCl_3 \rightarrow Ar + CHCl_2^+ + Cl + e^-$ was directly observed at an average collision energy of 0.13 eV using the oriented $CHCl_3$ molecular beam. The product $CHCl_2^+$ ions are measured for the H-end, the CCl_3-end, and sideways orientations. The obtained steric opacity function reveals that the CCl_3-end orientation is more favorable than the H-end orientation, and the sideways approach is found to be more favorable than the collinear approaches from both ends of the molecule. Furthermore, we confirm the good correlation between Penning ionization anisotropy and the electron density distribution of $2a_2$ HOMO orbital of $CHCl_3$ molecule, whose electron cloud is mostly localized around the sideways. These results substantiate the electron exchange mechanism which is commonly accepted for Penning ionization reaction, where the overlap of projectile atomic and target molecular orbital plays a key role in Penning ionization efficiency.

V-P-3 Hydrogen Adsorption and Reaction on the Ir{100}-(1×5) Surface

MORITANI, Kousuke[1]; OKADA, Michio[1]; KASAI, Toshio[2]; MURATA, Yoshitada[3]
([1]Osaka Univ.; [2]IMS and Osaka Univ.; [3]Univ. Electro-Commun.)

[*Surf. Sci.* **445**, 315 (2000)]

Adsorption of hydrogen (deuterium) on the Ir{100} surface has been studied with low-energy electron diffraction (LEED) and temperature-programmed desorption (TPD). At least three well-defined peaks can be identified with peak temperatures (T_p) of 125, 240, and 375 K in the TPD spectrum for the surface saturated with H at ~100 K. From the LEED observations, it can be concluded that these three peaks in the TPD spectrum correspond to H_2 desorption from the (1×5), (1×3), and (1×1) restructured phases, respectively. Furthermore, the result suggests that a metastable state of (1×3) exists on the Ir{100} surface in addition to the (1×1) phase. The series of TPD spectra for coadsorption of H_2 and D_2 on the Ir{100} surface show that an energetic D(H) atom produced in the dissociation process of incident $D_2(H_2)$ replaces a preadsorbed H(D) atom via energy transfer and the expelled H(D) atom moves to another adsorption site.

V-P-4 Hot Atom Mechanism in Hydrogen Exchange Reaction on the Ir{100} Surface

OKADA, Michio[1]; MORITANI, Kousuke[1]; NAKAMURA, Mamiko[1]; KASAI, Toshio[2]; MURATA, Yoshitada[3]
([1]Osaka Univ.; [2]IMS and Osaka Univ.; [3]Univ. Electro-Commun.)

[*Chem. Phys. Lett.* **323**, 586 (2000)]

H_2 exposure was found to induce the desorption of HD and D_2 molecules from the D-precovered Ir{100} surface. This result suggests that energetic H atoms (hot H atoms) produced in the dissociation process of incident H_s molecules react with preadsorbed D atoms and desorb as HD molecules or produce secondary energetic D atoms via energy transfer. Secondary energetic D atoms (secondary hot D atoms) also induce the associative reactions with preadsorbed D atoms and desorb as D_2 molecules.

V-Q Millimeter-Wave Spectroscopy Combined with Pulsed-Jet Expansion Technique for the Detection of the Novel Unstable Species and the van der Waals Mode Transitions of Molecular Clusters

Molecular clusters have inherently low-frequency vibrations, so called van der Waals (vdW) vibrational modes, which are characteristic of the weakly bound complexes. The frequency of the vdW mode usually falls in the far-infrared region (30–300 cm^{-1}). However, if a cluster is extremely floppy, it sometimes falls in the submillimeter-wave (SMMW) region below 30 cm^{-1}.

In this project, a millimeter-wave absorption spectrometer combined with pulsed-jet expansion technique has been devised and applied to the direct observation of the rovibrational transitions of the vdW bending band of molecular clusters. We have applied this technique to observe the vdW bending bands of the Ar–HCN (j = 1–0 and 2–1) and Ar–DCN (j = 1–0) clusters as well as the Ar–HBr (Σ_1–Σ_0) and OCO–HF (1^1–0^0 ($\nu_b{}^1$)) clusters. In this year, we have extended our measurements to the clusters as He–HCN, Ne–HCN, H_2–HCN, and H_2–H_2O. To increase the detection sensitivity, we employed a White-type multi-reflection optical system in the millimeter-wave region. The radiation was focused 20 times on the jet beam, and the improved sensitivity (of about one order of magnitude) was attained than the previous single path measurement.

The He–HCN cluster, for example, is a very weakly bound cluster with a binding energy of only 9 cm^{-1}. We have observed a number of j = 1–0 vdW transitions in 95–125 GHz and several observed levels are very close to the dissociation limit. The HCN part behave almost like a free rotor and dissociate with the excitation of vdW bending mode. The anisotropic intermolecular potential was determined by the least square fitting of the observed transitions.

The H_2–HCN, and H_2–H_2O clusters have rather complicated energy levels, because they have two internal rotors in the cluster, although the H_2 part behaves as a free rotor. Due to the spin statistics, the clusters have different internal rotation states between *para* and *ortho*-H_2 species, thus different dissociation energies, structures and vdW bending frequencies. The observed vdW transitions were analyzed to discuss the potential energy surface around HCN and H_2O.

In the supersonic jet expansions short lived species can survive thanks to the collision-less environment and ultra low rotational as well as vibrational temperature. The millimeter-wave spectrometer combined with supersonic jet nozzle and glow discharge electrodes, as well as the UV excimer laser photolysis devices, also have been set up for the detection of novel unstable species, such as radicals, molecular ions, and ionic and radical clusters.

V-Q-1 Millimeter-Wave Spectroscopy of the van der Waals Bending Band of He–HCN

HARADA, Kensuke; WHITHAM, Christopher J.; TANAKA, Keiichi[1]
([1]IMS and Kyushu Univ.)

The He–HCN cluster is a quite weakly bound cluster with the binding energy D_0 of 9 cm^{-1}.[1,2] The HCN part is almost freely rotating in the cluster. Recently two vdW bending transitions have been reported by molecular beam electric resonance technique.[1] The observation of the vdW transitions up to the dissociation limit is quite important for the determination of the potential energy surface and the theoretical analysis of the potential energy surface and intermolecular dynamics. In the present work, we observed the vdW bending transitions of the He–HCN cluster up to the dissociation limit and determined the empirical intermolecular potential function.

The multi-reflection millimeter wave jet cell was used for the experiment. The 14 atm mixed gas of 0.3% HCN and 99.7% He was injected to the vacuum chamber from a pulsed nozzle with a repetition rate of 60 Hz. The vacuum chamber was evacuated by a 10 inch diffusion pump. The millimeter wave radiation from a backward wave oscillator was passed twenty times through the jet expansion using a White type optical path and detected by InSb detector.

The energy level of He–HCN is labeled by the quantum numbers of j, l, and J where j is the internal rotation quantum number of HCN part, l is the rotational quantum number of the pseudo-diatomic complex and J is the total rotational quantum number. The stick diagram of the observed vdW transitions of He–HCN is shown in Figure 1. The 13 vdW bending transitions with $\Delta l = 0$ and $l = 0$~4 have been assigned in the frequency region of 95–125 GHz. The Q branch transitions and part of the R branch transitions are split to the hyperfine components due to the nuclear quadrupole interaction of the nitrogen nucleus. The highest observed energy level is the $j = 1$, $l = 4$, $J = 5$ level which is predicted to locate 0.5 cm^{-1} below the dissociation limit from the semi-empirical potential analysis.[2]

We used the one dimensional internal rotation Hamiltonian with the anisotropic intermolecular potential for the analysis. The potential function determined is shown in Figure 2. The angle between the HCN axis and the cluster axis is denoted by θ. The intermolecular potential $V(\theta)$ has a global minimum at $\theta = 0°$ (the linear structure of He–HCN) and the energy difference between $\theta = 0°$and $\theta = 180°$ (the linear structure of He–NCH) is 6 cm^{-1}. The center of mass distance R of He and HCN is 4.3 Å at $\theta = 0°$, while it is 0.8 Å shorter at $\theta = 70°$ than that at $\theta = 0°$.

References

1) S. Drucker, F. Tao and W. Klemperer, *J. Phys. Chem.* **99**, 2646 (1995).
2) K. M. Atkins and J. M. Hutson, *J. Chem. Phys.* **105**, 440 (1996).

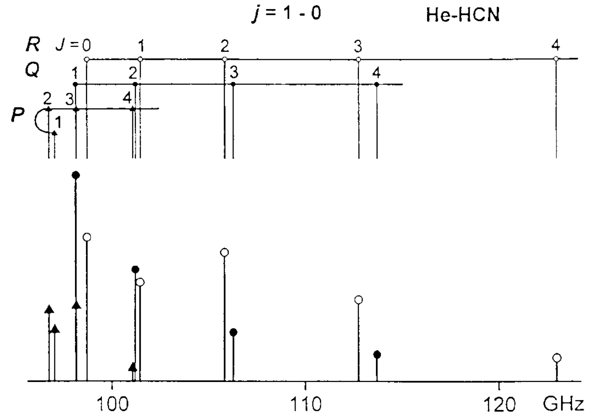

Figure 1. The stick diagram of the observed vdW bending transitions of He–HCN.

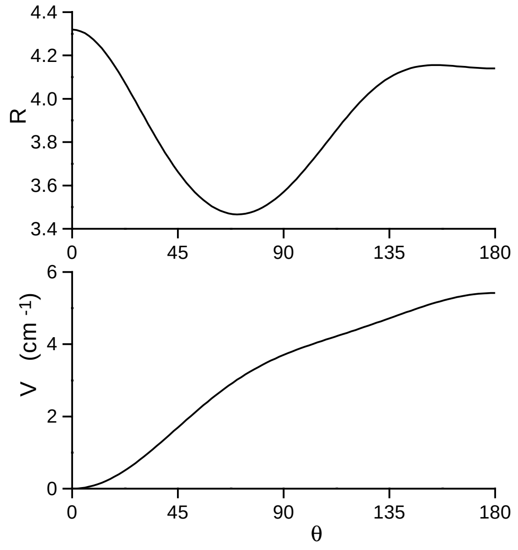

Figure 2. The *R*-θ and *V*-θ dependence curve of He–HCN.

V-Q-2 Millimeter Wave Spectroscopy of the HCN–H_2 Cluster

ISHIGURO, Masazumi[1]; WHITHAM, Christopher J.; HARADA, Kensuke; TANAKA, Takehiko[1]; TANAKA, Keiichi[2]
([1]Kyushu Univ.; [2]IMS and Kyushu Univ.)

Hydrogen H_2 containing molecular clusters are very weakly bound having large amplitude motion of both H_2 and its partner and they could have different configurations of between *para* (j = 0) and *ortho* (j = 1) hydrogen species. Recently, vibrational spectrum in the superfluid He droplets and ro-vibrational spectrum in the gas phase for the HCN–H_2 clusters have been observed. Vibrational spectrum in the He droplets suggests that o-H_2 binds to the N site of HCN molecule. Contrastedly, p-H_2 binds to the H site of HCN.1) In the gas phase, only HCN-(o-H_2) was detected.2) In this work, millimeter-wave absorption spectroscopy combined with a pulsed-jet expansion technique was applied to the measurement of the pure rotational and rovibrational transitions of the van der Waals (vdW) bending band of the HCN–H_2 cluster in the 75–150 GHz region.

So far, four rotational lines (J = 3–2 to 6–5) for the ground Σ_0 state of the HCN–(o-H_2) cluster split into hyperfine structure due to the nitrogen nucleus were observed. Rotational constant B_0 = 12899.718(20) MHz and centrifugal distortion constant D_0 = 12.2470(16) MHz were derived together with its higher order constants. The hyperfine constants determined eqQ = –2.830(33) MHz which is smaller than that of HCN molecule means a large amplitude motion of HCN <θ> = 31.1° in the ground linear form. The bond length between HCN and H_2 parts is derived to be 3.90 Å. This value strongly suggests that o-H_2 is bonding to the N site of the HCN molecule in the gas phase.

Some lines belonging to the Σ_1–Σ_0 vdW bending band of HCN–(o-H_2) were also observed. The Σ_1–Σ_0 vdW bending frequency 136.831 GHz of HCN–(o-H_2) is larger than that of He–HCN 96.8 GHz, but much smaller than that of Ar–HCN 164.89 GHz. The hyperfine constant in the Σ_1 state indicate the cluster has T-shape in the excited state of the vdW bending mode.

References

1) M. Ishiguro and R. E. Miller, *55th International Symposium on Molecular Spectroscopy* MF02, Ohio, 2000.
2) M. Ishiguro and R. E. Miller, *55th International Symposium on Molecular Spectroscopy* MF03, Ohio, 2000.

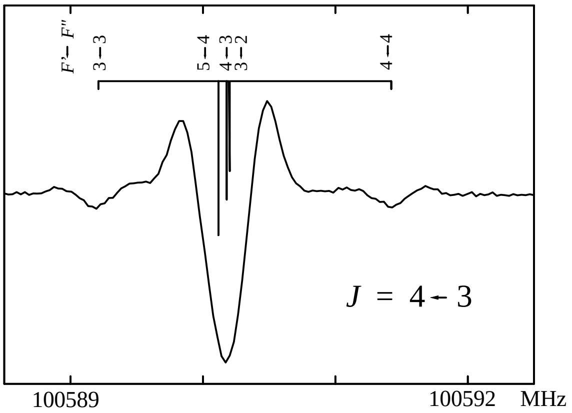

Figure 1. The J = 3–4 rotational line of the HCN–(o-H_2) in the ground Σ_0 state.

V-Q-3 Millimeter Wave Spectra of the H_2–H_2O van der Waals Complex

WHITHAM, Christopher J.; HARADA, Kensuke; TANAKA, Keiichi[1]
([1]IMS and Kyushu Univ.)

The hydrogen-water system is of interest due to the lightness (ie large rotational constants) of both parts which means that quantum dynamics effects are very important. High resolution spectra of such systems is helpful in developing models of the dynamics which include internal rotations of both partners.1) In addition, hydrogen–water collisions are believed to be important in the astronomical observations of intense water maser radiation.2) A recent infrared study of H_2–H_2O provided the motivation for this study.3)

We have observed pure rotational transitions of the weakly bound H_2–H_2O and H_2–D_2O complexes using a direct absorption millimeter wave spectrometer in the range 70–300 GHz. Internal rotation states involving ortho:H_2 (j = 1) Σ, ortho:H_2O $\Pi(1_{01})$ and para:H_2O $\Sigma(0_{00})$ were observed. The *e*/*f* parity splitting in the Π state provides important information on the intermolecular bending potential. Further work includes observation of the more weakly bound para:H_2–H_2O complex and direct excitation of the H_2O $\Sigma(1_{01})$–$\Pi(1_{01})$ transition which is predicted to lie in the 350 GHz region.

References

1) D. C. Clary and P. J. Knowles, *J. Chem. Phys.* **93**, 6334 (1990).
2) T. R. Phillips, S. Maluendes, A. D. McLean and S. Green, *J. Chem. Phys.* **101**, 5824 (1994).
3) M. J. Weida and D. J. Nesbitt, *J. Chem. Phys.* **110**, 156 (1999).

Table 1. Table of observed rotational transitions (MHz).

		H_2–H_2O	
J_{upper}–J_{lower}	$\Pi_e(1_{01})$	$\Pi_f(1_{01})$	$\Sigma(0_{00})$
2–1	71683.66	84983.56	85793.39
3–2	108760.57	126875.70	128002.72
4–3	146471.39	168017.75	169333.54
5–4	184341.19	208103.49	209391.38
		H_2–D_2O	
2–1	70684.54	82151.76	84412.97
3–2	106026.81	122766.98	126060.49
4–3	143955.50	162801.07	167009.37
5–4		202008.61	206976.05

V-Q-4 Millimeter Wave Spectroscopy of the van der Waals Bending Band of OCO-DF Generated in a Supersonic Jet Expansion

WHITHAM, Christopher J.; HARADA, Kensuke; ISHIGURO, Masazumi[1]; TANAKA, Takehiko[1]; TANAKA, Keiichi[2]
([1]Kyushu Univ.; [2]IMS and Kyushu Univ.)

The OCO–HF is a hydrogen-bonded quasi-linear cluster with a dissociation energy of 672 cm^{-1}.[1)] The inter molecular potential has minima at a bend structure of the COH angle of 22° and ~10 cm^{-1} potential barrier is expected at the linear structure of OCO-HF.[2)] In the preceding work, we have measured the van der Waals (vdW) bending band of OCO–HF directly by the millimeter wave jet spectroscopy. As a result, the vibrational frequency of vdW bending mode of OCO–HF has been determined precisely to be 272548.8017(49) MHz. To determine the complicated two dimensional inter molecular potential function with the COH bending and the OHF bending vibrations, it is important to observe vdW bending mode of OCO–DF as well as OCO–HF. In the present work, we have measured the vdW bending band of OCO–DF by the millimeter wave jet spectroscopy.

The 10 atm mixed gas of 1% DF, 5% CO_2, 31% Ar, and 63% Ne was injected to the vacuum chamber by the pulsed nozzle. We have measured 235–315 GHz region. The 31 rovibrational transitions of $P(2)$–$P(4)$, $Q(1)$–$Q(15)$, and $R(0)$–$R(12)$ were assigned to the 1^1–0^0 ($\nu_b{}^l$) fundamental band of the lowest vdW bending mode. The spectral pattern for OCO–DF was almost same as OCO–HF. The band has intense *Q* and *R* branch lines, while the *P* branch lines were rather weak. Figure 1 shows the fast scan spectrum of the band head of *Q* branch.

The usual linear molecule Hamiltonian with the rotational energy and the (2,2) interaction energy was used for the analysis. The band origin of the 1^1–0^0 ($\nu_b{}^l$) band has been determined to be 255815.6639(31) MHz, which is 6.1% smaller than that of OCO–HF. Furthermore, the rotational constant, centrifugal distortion constant, *l*-type doubling constant, and its higher order term were determined precisely. The analysis of the intermolecular potential function is now underway. In order to determine the precise two dimensional intermolecular bending potential surface, the measurement of the van der Waals hot band will be important.

References

1) L. Oudejans and R. E. Miller, *J. Chem. Phys.* **109**, 3474 (1998).
2) D. J. Nesbit and C. M. Lovejoy, *J. Chem. Phys.* **96**, 5712 (1992).

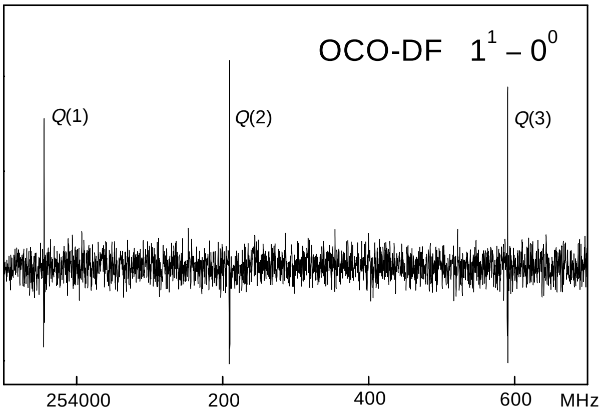

Figure 1. Fast scan spectrum of the head of *Q* branch for the OCO–DF.

V-R Ion-Molecule Reactions in the Troposphere

Ion chemistry in the troposphere is the most complicated among all level of earth's atmosphere because of the presence of a variety of trace compounds. We have studied ion-molecule reactions in the troposphere by investigating ion mobility distribution and its dependence on reaction time, pressure and temperature using an ion mobility spectrometer.[1,2] In order to confirm the ion-molecule reactions occurring in the troposphere, we have developed a high-resolution ion mobility/mass spectrometer which is capable of chemical identification of ion species forming ion peaks in mobility spectra. Using this spectrometer, we have been investigating the ion processes in conditioned laboratory air as well as in natural air. Experiments have been extended to the study on the role of ion-induced nucleation in the troposphere.

References

1) K. Nagato and T. Ogawa, *J. Geophys. Res.* **103**, 13917 (1998).
2) K. Nagato, D. J. Tanner, H. R. Friedli and F. L. Eisele, *J. Geophys. Res.* **104**, 3471 (1999).

V-R-1 Measurements of Mobility and Mass Spectra of Tropospheric Ions

NAGATO, Kenkichi

[*J. Aerosol Res. Jpn.* **15**, 110 (2000)]

An ion mobility/mass spectrometer (Figure 1) has been developed for the purpose of investigating the ion evolution in the lower troposphere. Total ion mobility spectra, mass spectra, and mass-resolved mobility spectra were obtained for positive and negative ions produced and aged for 0.02–0.5 s in the ambient air. In this range of aging time, positive ions were observed to evolve from $NH_4^+(H_2O)_n$ to the ions of pyridines and amines that have higher proton affinities. It is also demonstrated that mass-resolved mobility spectra could be useful to analyze the detailed pathway of the evolution. Four series of hydrated cluster ions were observed in the negative ion mass spectra, which are believed to be ions of formic acid ($HCOO^-(H_2O)_n$) and oxalic acid ($COOHCOO^-(H_2O)_n$) along with NO_2^--$(H_2O)_n$ and $NO_3^-(H_2O)_n$. This suggests that organic acids play important roles in the negative ion evolution in the lower troposphere.

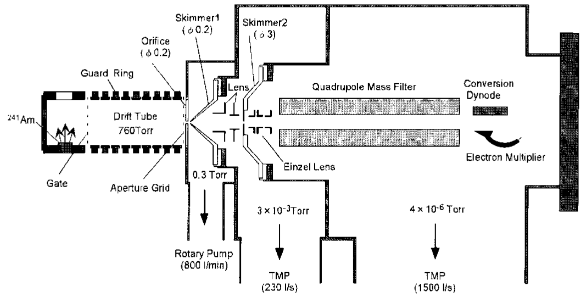

Figure 1. Schematic view of the ion mobility/mass spectrometer.

V-R-2 Experimental Study of Ion-Induced Nucleation in the Troposphere

NAGATO, Kenkichi; KIM, Chan Soo[1]; ADACHI, Motoaki[2]; OKUYAMA, Kikuo[1]
([1]Hiroshima Univ.; [2]Osaka Pref. Univ.)

There is a growing interest in the ion-induced nucleation in the troposphere.[1)] In order to investigate the role of tropospheric ions in the aerosol formation, measurements of mass spectra for positive and negative ions generated by α-ray radiolysis in the $NH_3/SO_2/H_2O$/Air mixture were made by using an ion mobility/mass spectrometer. In the negative ion mass spectra at low SO_2 and H_2O concentrations (Figure 1a), SO_2^-, SO_3^-, SO_4^-, and SO_5^- were observed as major SO_2-originated ions, which indicates that SO_2 were directly ionized by ion-molecule reactions. With increasing the concentrations of SO_2 and H_2O (Figure 1c), HSO_4^- and $HSO_4^-{\cdot}H_2SO_4$ ions became dominant, suggesting that SO_2 were primarily converted into H_2SO_4. This result agrees with our previous experiments that charged particle fraction decreased with increasing the concentrations of SO_2 and H_2O.[2,3)] It was also observed that the addition of NH_3 led the decrease in H_2SO_4.

References

1) F. Yu and R. P. Turco, *Geophys. Res. Lett.* **27**, 883 (2000).
2) T. O. Kim, *et al.*, *Aerosol Sci. Tech.* **26**, 527 (1997).
3) T. O. Kim, *et al.*, *Aerosol Sci. Tech.* **29**, 111 (1998).

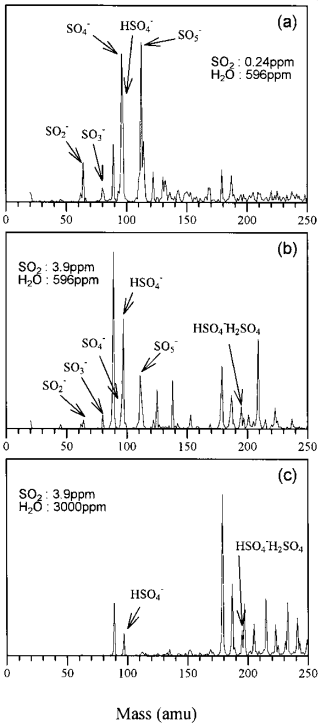

Figure 1. Mass spectra of negative ions generated by α-ray radiolysis in the SO_2/H_2O/Air mixture.

V-S Monte Carlo Simulation of Molecular Clusters

Physical properties of clusters have attracted much attention. Using Monte Carlo simulation methods, we investigate the properties of clusters and gels, helium in random potential, and other systems.

V-S-1 Boson Localization on the Superfluid-Insulator Transition by Quantum Loop Algorithm

HASHIMOTO, Masahito; TAKASU, Masako

[*Prog. Theor. Phys. Suppl.* **138** 529 (2000)]

For some systems in critical phenomena, Monte Carlo simulations using conventional algorithm is inefficient, because of strong correlation between successive MC configurations. Our system of helium in random potential suffers from this difficulty in critical region between superfluid phase and glass insulator phase. The loop algorithm overcomes this difficulty. We apply this algorithm to soft core boson system, and carry out calculations with random boson Hubbard model. This method is potentially useful for studying molecular clusters.

V-S-2 Monte Carlo Simulation of the Formation of Chemical Gel and Clusters

NOSAKA, Makoto; TAKASU, Masako

Gel is an important material used in everyday life. We focus our attention to the formation process of chemical gel and clusters. By changing the number of monomers, linkers and radicals, we obtain the phase diagram of gel. We also discuss efficient algorithm for determining the percolation of polymers.

V-S-3 Linear-shaped Motion of DNA in Concentrated Polymer Solutions Under a Steady Field

NOGUCHI, Hiroshi; TAKASU, Masako

[*J. Phys. Soc. Jpn.* submitted]

We studied the electrophoretic behavior of DNA chains in linear-polymer solutions using Brownian dynamics with an anisotropic friction tensor. We simulated the linear-shaped motion of DNA observed in highly concentrated solutions using a model with a chain segment equal to 1/4 of the persistence length. A linear conformation is seen for a chain with high segment-density regions, which remain at the same positions in space, with a high anisotropy of friction, while a U-shaped conformation is seen for a chain with a low anisotropy of friction.

V-T Development of Shaped Pulse Solid-State NMR Spectroscopy

Shaped radio frequency (rf) pulses are commonly employed in a solution high-resolution nuclear magnetic resonance (NMR) spectroscopy. They are used for selective excitation in multidimensional NMR experiments and broadband spin decoupling for resolution enhancements. However, they are less applied to solid state NMR experiments where the samples usually have much larger spectral widths than those of solution-state samples. In metallic or magnetic materials, the spin-echo method is still employed and only shifts and relaxation data are analyzed. Modern NMR techniques as a multiple quantum NMR provides a correlation of spin interactions between two nuclei, which seems to be very important even in these solid materials. We are currently developing a waveform generator and a transmission line probe, which enable excitations and detections of nuclear spins over a large spectral range.

V-T-1 Shaped Pulse Solid-State NMR Experiment

TAKAOKA, Kazuma[1]; ITOH, Toshiki[1]; KUBO, Atsushi; IMASHIRO, Fumio[1]; TERAO, Takehiko[1]
([1]Kyoto Univ.)

Shaped radio frequency (rf) pulses are commonly employed in a solution high-resolution nuclear magnetic resonance (NMR) spectroscopy. However, they are less applied to solid state NMR experiments where the samples usually show much larger spectral widths than those of solution-state samples. We have developed a fast wave form generator which could be employed for solid state shaped pulse experiments. Although the circuit was wired by cables on universal printed circuit boards, it worked stable to a clock frequency of 30 MHz. The waveform generator can be controlled by TTL signals from a spectrometer, and it can generate four different shaped pulses. We would like to publish our design elsewhere. We are also currently developing a transmission line probe,[1)] which may enables the broadband excitation of heavily broadened solid-state NMR spectra such as ^{195}Pt NMR of Pt nanoparticles. However, here we will demonstrate that the waveform generator is also useful in the experiments with an ordinary commercial NMR probe. Figure 1 (a) shows a ^{2}H solid-state magic-angle spinning NMR spectrum of a rigid deuterium sample with a quadrupole coupling of 160 kHz. An adiabatic inversion pulse WURST20[2)] was applied before the conventional observation pulse sequence and the result is shown in (b). The magnetization was inverted almost completely compared with (a), although the rf pulse amplitude was only 56 kHz. When a rectangular pulse with the same rf strength was used, only 40% of the magnetization were inverted. We conclude that adiabatic pulses may be promising, if it is difficult to obtain enough rf field strength, especially in triple-resonance experiments.

References
1) Conradi, M. S., *Concepts Magn. Reson.* **5**, 243 (1993).
2) Kupce, E.; Freeman, R., *J. Magn. Reson. A* **118**, 299 (1996).

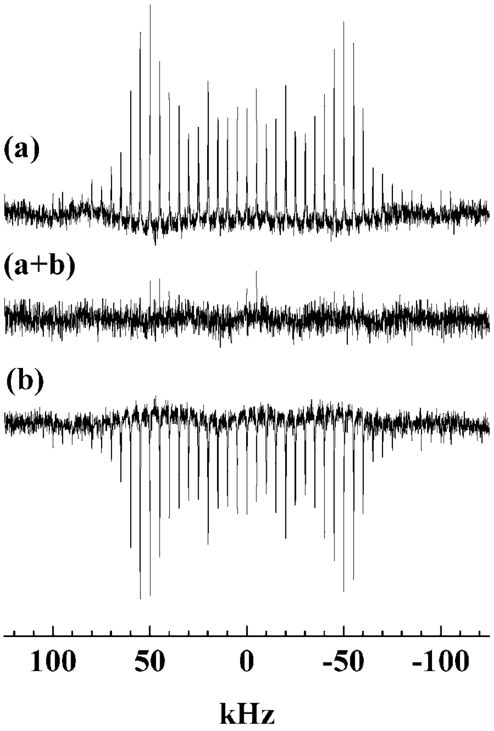

Figure 1. The inversion efficiencies of a ^{2}H magnetization by an adiabatic pulse, WURST20. (a) ^{2}H MAS NMR spectra of 2,2'-thiobis[5,5'-dimethyl-3-hydroxy-2-cyclohexen-1-one]-d_2. In (b), the magnetization was inverted by a WURST20 with length of 64 μs and a rf amplitude of 56 kHz. The rf frequency was swept during the pulse from –200 kHz to +200 kHz.

V-U Development of ^{13}C High-Resolution NMR Spectroscopy for Nematic and Cholesteric Liquid Crystals

When nematic and cholesteric liquid crystals are spun around a certain axis inclined from a static magnetic field, the directors of liquid crystals can be oriented in a perpendicular direction to the spinning axis. We have reported previously that ^{13}C NMR spectra recorded under this condition can be employed to determine a molecular diffusion rate along a pitch axis of a cholesteric liquid crystal (Y. Nishiyama, *et al., Mol. Phys.* **96**, 1569 (1999)). In the course of the study, we fortunately found a high-resolution two-dimensional NMR experiment, which correlates an isotropic chemical shift and a chemical shift anisotropy of nematic liquid crystals. This technique might be also applicable to determine structures of oriented biomacromolecules in a membrane.

V-U-1 Direct Determination of ^{13}C Chemical Shift Anisotropies of Liquid Crystals by Combining OMAS NMR and Rotor-Synchronous Pulses with Hankel Transformation

NISHIYAMA, Yusuke[1]; KUBO, Atsushi; TERAO, Takehiko[1]
([1]Kyoto Univ.)

The chemical shift anisotropies of liquid crystals are directly determined by a rotor-synchronous π pulse train under off-magic-angle spinning (OMAS). Using chemical shift anisotropies, we can determine the ^{13}C NMR peak correlations between a liquid crystalline phase and an isotropic phase. These peak correlations directly enable us to assign the spectrum of a liquid crystalline phase from the assignments for an isotropic phase. When a liquid crystal with a positive (negative) magnetic susceptibility anisotropy is spun around the axis inclined from the static magnetic filed by the angle ε larger (smaller) than the magic angle, the directors are randomly distributed in a plane perpendicular to the spinning axis. The orientation dependence of NMR resonance frequency vanishes by the spinning averaging over a half-rotor cycle. A rotor-synchronous π pulse re-introduces the orientation dependence, and the resulting free induction decay (FID) is expressed by the 0th Bessel function of the first kind $J_0(2C_2t/\pi)$, where C_2 is a coefficient related to the chemical shift anisotropy. The value of $|C_2|$ is determined by the Hankel transformation of the FID. The sign of C_2 is determined from a tilted 2D spectrum or from slices of 2D spectra recorded at two different angles ε. The property of the Hankel transformation is discussed. These theoretical results were verified by ^{13}C OMAS experiments with a π pulse train on a nematic liquid crystal of *p*-methoxy-benzilidene-*p*-n-butylaniline (MBBA).

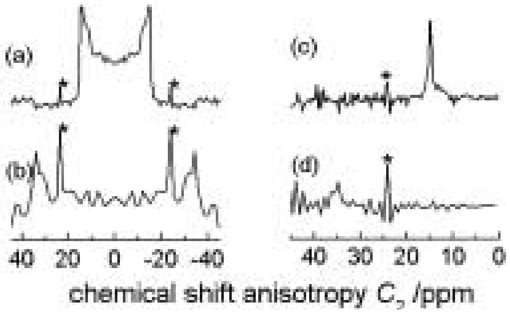

Figure 1. Comparisons between (a, b) Fourier transformed and (c, d) Hankel transformed spectra of MBBA at 302 K. The upper spectra (a, c) represent carbon-1 at 120.3 ppm and The lower spectra (b, d) represent carbon-9 at 175.1 ppm. The asterisks indicate the cycling sidebands due to the XY-8 phase cycling.